Journal of Vibration Engineering & Technologies (2026) 14:241
https://doi.org/10.1007/s42417-025-02172-2

ORIGINAL PAPER

Non-linear Aeroelastic Oscillations in Curvilinear Fibre-Reinforced Composite Cylindrical Shells

Pedro Ribeiro[1] · **Roeland de Breuker**[2]

Received: 31 July 2025 / Revised: 15 October 2025 / Accepted: 16 October 2025

Abstract

Purpose This study investigates how curvilinear fibre paths in variable stiffness composite laminates (VSCLs) influence large-amplitude, non-linear aeroelastic oscillations—particularly limit-cycle oscillations (LCOs) and chaotic responses—of circular cylindrical shells under supersonic flow. The aim is to assess whether curvilinear fibre reinforcements offer stability and performance advantages over traditional straight-fibre laminates in post-flutter regimes.

Methods A new geometrically non-linear model for circular cylindrical shells reinforced by curvilinear fibres is developed. It uses Kirchhoff's hypothesis and von Kármán strain–displacement relations, with the curvilinear fibre paths influencing the stiffness related terms. A single-element computational model incorporating polynomial and trigonometric basis functions enables efficient dynamic analysis. Linear stability is assessed via eigensolution routines, and post-flutter non-linear responses are obtained by time domain integration, where advantage is taken of the naturally reduced-order model.

Results The study finds that while the circumferential component of membrane inertia significantly affects certain vibration and flutter modes, longitudinal inertia can be neglected. Curvilinear fibre configurations delay flutter onset and modify the post-flutter response. Both LCOs and chaotic oscillations are observed, with curvilinear fibres shown to reduce oscillation amplitudes and lower frequency content in LCOs. Longitudinally travelling waves are identified and it is found that non-linear modal interaction is connected with chaotic behaviour.

Conclusion Curvilinear fibre orientations enhance the aeroelastic performance of cylindrical shells by extending the stable operating range before flutter occurs and by reducing the severity of post-flutter oscillations. These findings suggest that the use of curvilinear reinforcement fibres enables improvements in the non-linear dynamic behaviour of aerospace circular cylindrical thin structures.

Keywords Cylindrical shells · Variable stiffness composite laminate · Flutter · Non-linear analysis

Introduction

Aeroelastic phenomena involve significant mutual interaction among inertial, elastic and aerodynamic forces [1]. Of particular concern in aeroelasticity are two types of instabilities: divergence and flutter. Divergence occurs when, due to aeroelastic effects, the original equilibrium configuration of a structure loses stability and new, deformed, static equilibrium states are adopted. In the flutter case, static equilibrium gives rise to oscillations [1]. Both instabilities can lead to structural failure or to unexpected behaviour. The study of aeroelastic stability of circular cylindrical shells in axial flow [2] provides an academic testbed that is relevant for aerospace structures, such as fuselages, payload fairings and rockets [3–6].

In laminates where curvilinear fibres reinforce a resinous, polymeric matrix, the stress–strain relationship varies in the laminate domain. This is a type of Variable Stiffness Composite Laminate (VSCL). Material properties that dictate stiffness of the structure are fundamental in aeroelasticity. This paper focuses on how curvilinear reinforcement fibres affect the aeroelastic large amplitude oscillations that develop after flutter occurs in circular cylindrical shells.

Curvilinear fibres expanded the design domain and opened a field of research, leading to several publications

✉ Pedro Ribeiro
pmleal@fe.up.pt

[1] DEMec/INEGI, Faculdade de Engenharia, Universidade Do Porto, R. Dr. Roberto Frias, S/N, 4200-465 Porto, Portugal

[2] Faculty of Aerospace Engineering, Delft University of Technology, Kluyverweg 1, 2629 HS Delft, Netherlands

Published online: 17 April 2026

on mechanics, design and manufacturing [7–11]. Tatting [12] presented one of the earliest analyses on axisymmetric VSCL shells, mostly focusing on buckling and optimisation. Blom and co-workers (e.g. [13, 14]) investigated cylindrical and conical shells, optimising their fundamental vibration frequency and critical buckling load while also addressing the influence of manufacturing flaws. The buckling behaviour of cylindrical shells with curvilinear fibres was further explored in [15–17], with [15] and [16] containing experimental data from buckling and vibrations tests. In [18], an optimization framework based on metamodels was developed with the goal of minimizing the mass of variable-angle filament-wound cylinders. More recently, Kumar and Hirwani [19] developed a higher-order finite element model to investigate the geometrically non-linear vibrations of VSCL shell panels, incorporating Green–Lagrange strains and exploring the effects of fibre orientation, boundary conditions and material parameters on transient responses. These works illustrate relevant research directions on VSCL shells, encompassing studies on buckling and vibration, optimisation strategies and advanced modelling approaches, but none of them addresses post-flutter behaviour.

Although post-flutter behaviour has not been analysed in VSCL shells, a few studies on isotropic and constant stiffness laminated circular cylindrical shells highlight the significance of analysing this regime. Amabili and Pellicano [20, 21], for example, included geometric non-linearities in the study of supersonic flutter of circular cylindrical shells, using a theory designated as “Donnell’s non[-]linear shallow-shell theory”. Travelling-waves were found in the first study and axisymmetric imperfections were included in the second. In [22], linear Sander’s shell theory was employed to derive a finite element for circular cylindrical shells and the onset of flutter was analysed. Composite laminated circular cylindrical shells under the combined action of radial harmonic excitation, compressive in-plane force and aerodynamic pressure were studied in [23]. Yacine et al. [24] present a numerical model, which adopts exact solutions of linear Sander’s theory as displacement functions, to study the impact of geometric non-linearities and diverse parameters on the dynamic behaviour of thin cylindrical shells subjected to supersonic flow.

To conclude this literature review, studies related to applications of variable stiffness materials in aeroelastic problems are mentioned. A high-aspect-ratio wingbox with tow-steered wing skins was designed, manufactured, and tested as part of the NASA Advanced Air Transport Technology Project (AATT), as described in [25] and [26]. The tow-steered wing skins were designed to improve fuel efficiency under aeroelastic loads. Curvilinear fibre tailoring of plates, shells, and wings to enhance aeroelastic characteristics has been researched in [27–33].

The literature review indicates that using curvilinear fibres may be beneficial in *after-flutter* large amplitude oscillations of circular cylindrical shells. However, this problem has not been addressed to date. The present analysis aims to bridge this gap, providing a more comprehensive understanding of the dynamics of VSCL circular cylindrical shells under supersonic flow, and to evaluate the potential of curvilinear fibres. It includes the development of a new mathematical model for this problem and an evaluation of different model condensation alternatives. Reduced models are particularly relevant for non-linear computations and parametric studies.

The original full model is described in Sect. "Equations of Motion – Full Model", with lengthy mathematical details provided in an appendix. A linear piston theory, which is able to represent aerodynamic forces at specific Mach numbers [1, 2], is employed. For the structural model, an equivalent single layer theory based on Kirchhoff’s hypothesis [2] is preferred, because priority is here given to the analysis of thin panels and this theory leads to computationally efficient models. When flutter develops, the shells undergo large amplitude oscillations [1, 34], requiring the use of a geometrically non-linear structural model. This is achieved using strain–displacement relations of the von Kármán type [2]. Galerkin’s method [35, 36] is then applied to obtain Non-Linear Ordinary Differential Equations of motion, which are solved in the time domain.

In Sect. "Equations of Motion – reduced-order Models" of the paper, two types of reduced-order models are presented. Sect. "Linear Aeroelastic Dtability" briefly describes how aeroelastic stability is studied in the linear domain. Convergence and validation studies are presented at the beginning of Sect. "Hopf Bifurcations and Non-linear Oscillations of VSCL Shells" and in an appendix. The features of the full and two reduced-order models are analysed. Subsequently, in the remainder of Sect. "Hopf Bifurcations and Non-linear Oscillations of VSCL Shells", the non-linear dynamics of VSCL shells under supersonic flows are examined and compared to those of a reference constant stiffness shell. In addition to nearly harmonic oscillations, periodic, but far from harmonic, and chaotic oscillations are found. The effect that travelling waves have on the shells displacements is illustrated. It is shown that curvilinear fibre paths allow decreasing the amplitudes of flutter-induced oscillations and increasing the pressure range within which stable limit cycle oscillations occur. Finally, Sect. 6 closes the paper with a summary of the findings.

Equations of Motion – Full Model

The length (ℓ), radius of the middle surface (R) and thickness (h) of a cylindrical shell are represented in Fig. 1, as well as the cylindrical coordinates.

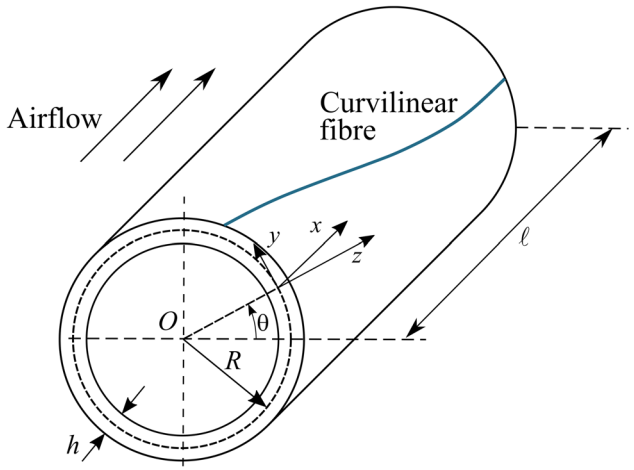

Fig. 1 Dimensions and coordinate system of a cylindrical shell. θ is measured anticlockwise so that increasing θ corresponds to positive y

The mathematical/theoretical model now presented is based on Kirchhoff's hypothesis, supplemented with strain displacement relations of the von Kármán type (given further down) to account for moderately large displacements [2, 37]. Hence, the displacement components in directions x, y and z (Cartesian coordinate system in Fig. 1), are, respectively, written as follows

$$\begin{aligned} u(x,\theta,z,t) &= u_0(x,\theta,t) - z\frac{\partial w_0(x,\theta,t)}{\partial x} \\ v(x,\theta,z,t) &= v_0(x,\theta,t) - \frac{z}{R}\frac{\partial w_0(x,\theta,t)}{\partial \theta} \\ w(x,\theta,z,t) &= w_0(x,\theta,t) \end{aligned} \tag{1}$$

where subscript $_0$ denotes the middle surface.

Equations of motion in stress resultants

Mass distribution is considered to be homogeneous and the external force per unit area, represented by $p_z(x, \theta, t)$, is perpendicular to the shell's surface. The dynamic equilibrium equations can be written adding membrane terms due to geometrical non-linearity to the linear equations of motion given in [38, 39],[1]

$$\frac{\partial N_{xx}(x,\theta,t)}{\partial x} + \frac{1}{R}\frac{\partial N_{x\theta}(x,\theta,t)}{\partial \theta} = \rho h \frac{\partial^2 u_0(x,\theta,t)}{\partial t^2}, \tag{2}$$

$$\begin{aligned} &\frac{1}{R}\frac{\partial N_{\theta\theta}(x,\theta,t)}{\partial \theta} + \frac{\partial N_{x\theta}(x,\theta,t)}{\partial x} \\ &+ \frac{1}{R}\left(\frac{1}{R}\frac{\partial M_{\theta\theta}(x,\theta,t)}{\partial \theta} + \frac{\partial M_{x\theta}(x,\theta,t)}{\partial x}\right) \\ &= \rho h \frac{\partial^2 v_0(x,\theta,t)}{\partial t^2}, \end{aligned} \tag{3}$$

$$\begin{aligned} &-\frac{N_{\theta\theta}(x,\theta,t)}{R} + N_{nlin}(x,\theta,t) + \frac{\partial^2 M_{xx}(x,\theta,t)}{\partial x^2} \\ &+ \frac{2}{R}\frac{\partial^2 M_{x\theta}(x,\theta,t)}{\partial \theta \partial x} + \frac{1}{R^2}\frac{\partial^2 M_{\theta\theta}(x,\theta,t)}{\partial \theta^2} + \\ &p_z(x,\theta,t) = \rho h \frac{\partial^2 w_0(x,\theta,t)}{\partial t^2}. \end{aligned} \tag{4}$$

The non-linearity due to large displacements leads to the following term

$$\begin{aligned} N_{nlinear} &= \frac{\partial}{\partial x}\left(N_{xx}\frac{\partial w_0}{\partial x} + \frac{N_{x\theta}}{R}\frac{\partial w_0}{\partial \theta}\right) \\ &+ \frac{1}{R}\frac{\partial}{\partial \theta}\left(N_{x\theta}\frac{\partial w_0}{\partial x} + \frac{N_{\theta\theta}}{R}\frac{\partial w_0}{\partial \theta}\right). \end{aligned} \tag{5}$$

Equations (4) and (5) are similar Eq. (8) of [40]. Taking into account the different orientation of the z-axis, they also correspond to Eq. (1.152) of [2].

Stress resultants N_{xx}, $N_{\theta\theta}$ and $N_{x\theta}$ are membrane forces per unit length; terms M_{xx}, $M_{\theta\theta}$ and $M_{x\theta}$ are bending and twisting moments per unit length. They are the components of the vectors $\mathbf{N}$ and $\mathbf{M}$, which are related to the diverse components of strain, $\boldsymbol{\varepsilon}_0^m$ and $\boldsymbol{\varepsilon}_0^{nl}$, and to the components of the curvature change, $\boldsymbol{\chi}_0^b$, by

$$\mathbf{N} = \mathbf{A}\boldsymbol{\varepsilon}_0^m + \mathbf{A}\boldsymbol{\varepsilon}_0^{nl}, \tag{6}$$

$$\mathbf{M} = \mathbf{D}\boldsymbol{\chi}_0^b, \tag{7}$$

Matrices $\mathbf{A}$ and $\mathbf{D}$ contain the stiffness coefficients resulting from the piecewise integration through the shell thickness [38]. In this work, the material in each layer is assumed to be linear elastic and orthotropic. However, due to the variation of the fibre orientation—intrinsic to curvilinear fibres—the components of matrices $\mathbf{A}$ and $\mathbf{D}$ are not constant, they vary throughout the shell's domain. In this sense, the material of a single layer is not homogeneous on a macroscopic level. For a detailed derivation of these matrices for circular cylindrical shells with curvilinear fibres, the reader is referred to [31].

Vector $\boldsymbol{\varepsilon}_0^m$ contains the linear part of the membrane strains in the middle surface, and vector $\boldsymbol{\varepsilon}_0^{nl}$ contains the non-linear part.

$$\boldsymbol{\varepsilon}_0^m = \begin{Bmatrix} \frac{\partial u_0}{\partial x} \\ \frac{\partial v_0}{R\partial \theta} + \frac{w_0}{R} \\ \frac{\partial v_0}{\partial x} + \frac{1}{R}\frac{\partial u_0}{\partial \theta} \end{Bmatrix}, \tag{8}$$

$$\boldsymbol{\varepsilon}_0^{nl} = \begin{Bmatrix} \frac{1}{2}\left(\frac{\partial w_0}{\partial x}\right)^2 \\ \frac{1}{2}\left(\frac{1}{R}\frac{\partial w_0}{\partial \theta}\right)^2 \\ \frac{1}{R}\frac{\partial w_0}{\partial \theta}\frac{\partial w_0}{\partial x} \end{Bmatrix}. \tag{9}$$

[1] Specifically, the non-linear terms were added to Eqs. (7.6) of [38] Qatu MS. Vibration of Laminated Shells and Plates: Academic Press, 2004., with $a=x$, $\beta=R\theta$ and reverse signs in the inertia terms.

The curvature changes are placed in vector $\boldsymbol{\chi}_o^b$

$$\boldsymbol{\chi}_{\mathrm{o}}^{\mathrm{b}} = \left\{ \begin{array}{c} -\frac{\partial w_0^2}{\partial x^2} \\ \frac{1}{R^2}\frac{\partial v_0}{\partial \theta} - \frac{1}{R^2}\frac{\partial w_0^2}{\partial \theta^2} \\ \frac{1}{R}\frac{\partial v_0}{\partial x} - \frac{2}{R}\frac{\partial w_0^2}{\partial x \partial \theta} \end{array} \right\} \tag{10}$$

The terms $\frac{1}{R^2}\frac{\partial v_0}{\partial \theta}$ and $\frac{1}{R}\frac{\partial v_0}{\partial x}$ are generally small in comparison to those in w_0 and have therefore been neglected in Sect. 1.3.4 of [2] and in [40]. However, they are considered in Sect. 7.1.1 of [38] and will also be retained in this work, contributing to a slightly more accurate model with minimal additional computational effort. On the other hand, the term z/R is very small in comparison to unity ($R+z \cong R$) in thin shells and was therefore neglected. This customary simplification, consistent with thin shell theory, avoids unnecessary complexity in modelling.

For future reference, the forces and moments per unit length are now written in full

$$\begin{aligned} N_{xx} &= A_{11}\left[\frac{\partial u_0}{\partial x} + \frac{1}{2}\left(\frac{\partial w_0}{\partial x}\right)^2\right] \\ &+ A_{12}\left[\frac{1}{R}\frac{\partial v_0}{\partial \theta} + \frac{w_0}{R} + \frac{1}{2}\left(\frac{1}{R}\frac{\partial w_0}{\partial \theta}\right)^2\right] \\ &+ A_{16}\left(\frac{1}{R}\frac{\partial u_0}{\partial \theta} + \frac{\partial v_0}{\partial x} + \frac{1}{R}\frac{\partial w_0}{\partial \theta}\frac{\partial w_0}{\partial x}\right) \end{aligned} \tag{11}$$

$$\begin{aligned} N_{\theta\theta} &= A_{12}\left[\frac{\partial u_0}{\partial x} + \frac{1}{2}\left(\frac{\partial w_0}{\partial x}\right)^2\right] \\ &+ A_{22}\left[\frac{1}{R}\frac{\partial v_0}{\partial \theta} + \frac{w_0}{R} + \frac{1}{2}\left(\frac{1}{R}\frac{\partial w_0}{\partial \theta}\right)^2\right] \\ &+ A_{26}\left(\frac{1}{R}\frac{\partial u_0}{\partial \theta} + \frac{\partial v_0}{\partial x} + \frac{1}{R}\frac{\partial w_0}{\partial \theta}\frac{\partial w_0}{\partial x}\right) \end{aligned} \tag{12}$$

$$\begin{aligned} N_{x\theta} &= A_{16}\left[\frac{\partial u_0}{\partial x} + \frac{1}{2}\left(\frac{\partial w_0}{\partial x}\right)^2\right] \\ &+ A_{26}\left[\frac{1}{R}\frac{\partial v_0}{\partial \theta} + \frac{w_0}{R} + \frac{1}{2}\left(\frac{1}{R}\frac{\partial w_0}{\partial \theta}\right)^2\right] \\ &+ A_{66}\left(\frac{1}{R}\frac{\partial u_0}{\partial \theta} + \frac{\partial v_0}{\partial x} + \frac{1}{R}\frac{\partial w_0}{\partial \theta}\frac{\partial w_0}{\partial x}\right) \end{aligned} \tag{13}$$

$$\begin{aligned} M_{xx} &= -D_{11}\frac{\partial^2 w_0}{\partial x^2} + D_{12}\left(\frac{1}{R^2}\frac{\partial v_0}{\partial \theta}\right. \\ &\left. -\frac{1}{R^2}\frac{\partial^2 w_0}{\partial \theta^2}\right) + D_{16}\left(\frac{1}{R}\frac{\partial v_0}{\partial x} - \frac{2}{R}\frac{\partial^2 w_0}{\partial x \partial \theta}\right) \end{aligned} \tag{14}$$

$$\begin{aligned} M_{\theta\theta} &= -D_{21}\frac{\partial^2 w_0}{\partial x^2} + D_{22}\left(\frac{1}{R^2}\frac{\partial v_0}{\partial \theta}\right. \\ &\left. -\frac{1}{R^2}\frac{\partial^2 w_0}{\partial \theta^2}\right) + D_{26}\left(\frac{1}{R}\frac{\partial v_0}{\partial x} - \frac{2}{R}\frac{\partial^2 w_0}{\partial x \partial \theta}\right) \end{aligned} \tag{15}$$

$$\begin{aligned} M_{x\theta} &= -D_{16}\frac{\partial^2 w_0}{\partial x^2} + D_{26}\left(\frac{1}{R^2}\frac{\partial v_0}{\partial \theta}\right. \\ &\left. -\frac{1}{R^2}\frac{\partial^2 w_0}{\partial \theta^2}\right) + D_{66}\left(\frac{1}{R}\frac{\partial v_0}{\partial x} - \frac{2}{R}\frac{\partial^2 w_0}{\partial x \partial \theta}\right) \end{aligned} \tag{16}$$

Independent variables are omitted for brevity, but we recall that the stiffness coefficients A_{ij} and D_{ij} are functions of spatial coordinates. In this work, they depend solely on the longitudinal coordinate.

The approximation functions introduced later depend on non-dimensional coordinate ξ. By employing a single element to represent the entire shell, ξ is related to x by

$$x = \frac{\ell}{2}(\xi + 1), \tag{17}$$

with ℓ the shell length (Fig. 1).

Naturally, fewer restrictions on the fibre path expand the design domain and increase the potential to achieve better designs. However, more general fibre paths complicate the investigation and demand employing optimisation procedures. Although optimisation plays a significant role in research on variable stiffness composite laminates [7, 10], this study adopts a complementary approach, focusing on the modelling and analysis of the aeroelastic effects of curvilinear fibre paths. The insights achieved can inform and enhance future optimisation strategies. The following relation for the angle between the tangent to the fibre path and the longitudinal axis

$$\psi(\xi) = (\Theta_1 - \Theta_0) \cdot \frac{\xi + 1}{2} + \Theta_0 \tag{18}$$

is adequate for the aims of this research.It results from Eq. (18) that the fibre angle is equal to Θ_0 at $x=0$ ($\xi=-1$) and equal to Θ_1 at $x=\ell$ ($\xi=1$); a layer with this fibre path is represented as $<\Theta_0, \Theta_1>$.

Expression (18) was chosen because of its simplicity and because the fibre paths it defines led, in reference [31], to higher critical pressures then straight fibres and performed quite well in comparison with alternative curvilinear path types, recognising, nonetheless, that the constant curvature fibre path was also shown to have advantages. Using expressions like (18) guarantees a smooth fibre path that remains manufacturable as long as curvature constraints

are respected. Moreover, because the path is defined by solely two parameters, it facilitates iterative design exploration without an excessive computational burden. It is here assumed that all fibres are disposed respecting Eq. (18), which is not exactly the case. In practice, when Automatic Fibre Placement is employed [9, 11, 41, 42], the fibres tows follow paths parallel to the reference trajectory rather than respecting it exactly.

Displacement Approximation

The middle surface displacements are expanded as sums of products of spatial and time variables as follows

$$\begin{Bmatrix} u_0(\xi,\theta,t) \\ v_0(\xi,\theta,t) \\ w_0(\xi,\theta,t) \end{Bmatrix} = \begin{bmatrix} \mathbf{ff}^u(\xi,\theta)^{\mathbf{T}} & \mathbf{0} & \mathbf{0} \\ \mathbf{0} & \mathbf{ff}^v(\xi,\theta)^{\mathbf{T}} & \mathbf{0} \\ \mathbf{0} & \mathbf{0} & \mathbf{ff}^w(\xi,\theta)^{\mathbf{T}} \end{bmatrix} \begin{Bmatrix} \mathbf{q}_u(t) \\ \mathbf{q}_v(t) \\ \mathbf{q}_w(t) \end{Bmatrix}, \tag{19}$$

$\mathbf{ff}^i(\xi, \theta)$ ($i=u, v, w$) are vectors of shape or approximation functions; $\mathbf{q}_i(t)$ are vectors of generalized displacements. The shape functions in ξ and θ are defined by multiplying unidimensional shape functions of the two coordinates. For each displacement component, the total number of unidimensional shape functions along x is represented by p_j, where $j=\xi u, \xi v, \xi w$; the number of unidimensional circumferential shape functions is p_k, with $k= \theta u, \theta v, \theta w$. Therefore, for example, approximating the longitudinal membrane displacement components requires a total of $p_{\xi_u} \cdot p_{\theta_u}$ shape functions. The total number of shape functions employed in the full model is

$$n = np_u \cdot np_v \cdot np_w \tag{20}$$

where

$$\begin{aligned} &np_u = p_{\xi u} \cdot p_{\theta u}, np_v = p_{\xi v} \cdot \\ &p_{\theta v}, np_w = p_{\xi w} \cdot p_{\theta w}, n_{c2} = np_v + np_w \end{aligned} \tag{21}$$

n_{c2} is a parameter that will also be useful.

In this work, the shape functions along ξ are polynomials. For the displacement components u and v, polynomials from the same set are employed, denoted here by gu_i and gv_i, respectively. The polynomials used for the transverse displacement w are represented by fw_j. These two sets of polynomials allow easily respecting the geometric boundary conditions and can be found, for example, in [43–45]. Both sets of polynomials have been successfully applied numerous times, often in a p-version finite element method context [31, 43–47]. They require a relatively small number of degrees of freedom and computational times, and are less susceptible to numerical errors than other high order polynomials they have been compared to in vibration problems.

In the circumferential direction, the shape functions have to respect periodicity conditions, specifically, they should be continuous and so should be their derivative. Here, functions from the following sets are employed [23]

$$t_{u_k}(\theta) = t_{w_k}(\theta) = \cos((k-1)\theta), k \geq 1 \tag{22}$$

$$\begin{aligned} t_{v_1}(\theta) &= 1 && \Leftarrow k = 1 \\ t_{v_k}(\theta) &= \sin((k-1)\theta) && \Leftarrow k \geq 2 \end{aligned} \tag{23}$$

Cosine functions were also applied for the transverse displacement by Barr and Stearman in reference [6], where comparisons with experiments are presented. Nonetheless, sets (22) and (23) do not allow investigating travelling waves that may develop in the circumferential direction [3, 20]. For this purpose, orthogonal circumferential functions should be added to (22) and (23). The analysis of circumferential travelling waves in VSCL shells is not addressed here; it represents an extension of this work that can build on the model and findings of this study. On the other hand, the occurrence of longitudinal travelling waves will be exposed.

Ordinary Differential Equations of Motion

Equation (2) is multiplied by $g_{u_i} \cdot t_{u_m}$ and integration by parts is performed in ξ or θ, boundary conditions where either the longitudinal displacement component or the longitudinal force is null are considered. Similarly, Eqs. (3) and (4) are, respectively, multiplied by $g_{v_i} \cdot t_{v_m}$ and f_{w_m}, and integrations by parts are carried out. Boundary conditions that allow nullifying terms

evaluated at $\xi = \pm 1$ are assumed. This Galerkin procedure [35, 36] leads to the following three equations

$$\begin{aligned}
&\int_{-1}^{1}\int_{0}^{2\pi} \frac{\mathrm{d}g_{u_i}(\xi)}{\mathrm{d}\xi} t_{u_m}(\theta) N_{xx}(\xi,\theta,t) R \mathrm{d}\theta \mathrm{d}\xi \\
&+ \int_{-1}^{1}\int_{0}^{2\pi} g_{u_i}(\xi) \frac{\mathrm{d}t_{u_m}(\theta)}{\mathrm{d}\theta} N_{x\theta}(x,\theta,t) \frac{\ell}{2} \mathrm{d}\theta \mathrm{d}\xi \\
&= -\int_{-1}^{1}\int_{0}^{2\pi} g_{u_i}(\xi) t_{u_m}(\theta) \frac{\partial^2 u_0(x,\theta,t)}{\partial t^2} \rho h \frac{R\ell}{2} \mathrm{d}\theta \mathrm{d}\xi,
\end{aligned} \tag{24}$$

$$\begin{aligned}
&\int_{-1}^{1}\int_{0}^{2\pi} g_{v_i}(\xi) \frac{\mathrm{d}t_{v_m}(\theta)}{\mathrm{d}\theta} N_{\theta\theta}(\xi,\theta,t) \frac{\ell}{2} \mathrm{d}\theta \mathrm{d}\xi \\
&+ \int_{-1}^{1}\int_{0}^{2\pi} \frac{\mathrm{d}g_{v_i}(\xi)}{\mathrm{d}\xi} t_{v_m}(\theta) N_{x\theta}(\xi,\theta,t) R \mathrm{d}\theta \mathrm{d}\xi \\
&+ \int_{-1}^{1}\int_{0}^{2\pi} g_{v_i}(\xi) \frac{\mathrm{d}t_{v_m}(\theta)}{\mathrm{d}\theta} M_{\theta\theta}(\xi,\theta,t) \frac{1}{R}\frac{\ell}{2} \mathrm{d}\theta \mathrm{d}\xi \\
&+ \int_{-1}^{1}\int_{0}^{2\pi} \frac{\mathrm{d}g_{v_i}(\xi)}{\mathrm{d}\xi} t_{v_m}(\theta) M_{x\theta}(\xi,\theta,t) \mathrm{d}\theta \mathrm{d}\xi \\
&= -\int_{-1}^{1}\int_{0}^{2\pi} g_{v_i}(\xi) t_{v_m}(\theta) \frac{\partial^2 v_0(x,\theta,t)}{\partial t^2} \rho h \frac{R\ell}{2} \mathrm{d}\theta \mathrm{d}\xi,
\end{aligned} \tag{25}$$

$$\begin{aligned}
&\int_{-1}^{1}\int_{0}^{2\pi} - f_{w_i}(\xi) t_{w_m}(\theta) N_{\theta\theta}(x,\theta,t) \frac{\ell}{2} \mathrm{d}\theta \mathrm{d}\xi \\
&- \int_{-1}^{1}\int_{0}^{2\pi} \frac{\mathrm{d}f_{w_i}(\xi)}{\mathrm{d}\xi} t_{w_m}(\theta) N_{xx} \frac{\partial w_0}{\partial x} R \mathrm{d}\theta \mathrm{d}\xi \\
&- \int_{-1}^{1}\int_{0}^{2\pi} \frac{\mathrm{d}f_{w_i}(\xi)}{\mathrm{d}\xi} t_{w_m}(\theta) N_{x\theta} \frac{\partial w_0}{\partial \theta} \mathrm{d}\theta \mathrm{d}\xi \\
&- \int_{-1}^{1}\int_{0}^{2\pi} f_{w_i}(\xi) \frac{\mathrm{d}t_{w_m}(\theta)}{\mathrm{d}\theta} N_{x\theta} \frac{\partial w_0}{\partial x} \frac{\ell}{2} \mathrm{d}\theta \mathrm{d}\xi \\
&- \int_{-1}^{1}\int_{0}^{2\pi} f_{w_i}(\xi) \frac{\mathrm{d}t_{w_m}(\theta)}{\mathrm{d}\theta} N_{\theta\theta} \frac{\partial w_0}{\partial \theta} \frac{\ell}{2R} \mathrm{d}\theta \mathrm{d}\xi \\
&- \int_{-1}^{1}\int_{0}^{2\pi} \frac{\mathrm{d}f_{w_i}(\xi)}{\mathrm{d}\xi} t_{w_m}(\theta) \frac{\partial M_{xx}(x,\theta,t)}{\partial x} R \mathrm{d}\theta \mathrm{d}\xi + \\
&- \int_{-1}^{1}\int_{0}^{2\pi} \frac{\mathrm{d}f_{w_i}(\xi)}{\mathrm{d}\xi} t_{w_m}(\theta) \frac{\partial M_{x\theta}(x,\theta,t)}{\partial \theta} \mathrm{d}\theta \mathrm{d}\xi \\
&- \int_{-1}^{1}\int_{0}^{2\pi} f_{w_i}(\xi) \frac{\mathrm{d}t_{w_m}(\theta)}{\mathrm{d}\theta} \frac{\partial M_{x\theta}(x,\theta,t)}{\partial x} \frac{\ell}{2} \mathrm{d}\theta \mathrm{d}\xi \\
&- \int_{-1}^{1}\int_{0}^{2\pi} f_{w_i}(\xi) \frac{\mathrm{d}t_{w_m}(\theta)}{\mathrm{d}\theta} \frac{\partial M_{\theta\theta}(x,\theta,t)}{\partial \theta} \frac{\ell}{2R} \mathrm{d}\theta \mathrm{d}\xi \\
&+ \int_{-1}^{1}\int_{0}^{2\pi} f_{w_i}(\xi) t_{w_m}(\theta) p_z(x,\theta,t) \frac{R\ell}{2} \mathrm{d}\theta \mathrm{d}\xi \\
&= \int_{-1}^{1}\int_{0}^{2\pi} f_{w_i}(\xi) t_{w_m}(\theta) \frac{\partial^2 w_0(x,\theta,t)}{\partial t^2} \rho h \frac{R\ell}{2} \mathrm{d}\theta \mathrm{d}\xi
\end{aligned} \tag{26}$$

Using the expressions of forces and moments per unit length as functions of displacement components from (11) to (16), Eqs. (24) and (25) become, respectively,

$$\begin{aligned}
&\int_{-1}^{1}\int_{0}^{2\pi} \frac{\mathrm{d}g_{u_i}}{\mathrm{d}\xi} t_{u_m} \left\{ A_{11}\left[\frac{\partial u_0}{\partial x} + \frac{1}{2}\left(\frac{\partial w_0}{\partial x}\right)^2\right] + A_{12}\left[\frac{1}{R}\frac{\partial v_0}{\partial \theta} + \frac{w_0}{R} + \frac{1}{2}\left(\frac{1}{R}\frac{\partial w_0}{\partial \theta}\right)^2\right] + A_{16}\left(\frac{1}{R}\frac{\partial u_0}{\partial \theta} + \frac{\partial v_0}{\partial x} + \frac{1}{R}\frac{\partial w_0}{\partial \theta}\frac{\partial w_0}{\partial x}\right)\right\} R \mathrm{d}\theta \mathrm{d}\xi \\
&+ \int_{-1}^{1}\int_{0}^{2\pi} g_{u_i} \frac{\mathrm{d}t_{u_m}}{\mathrm{d}\theta} \left\{ A_{16}\left[\frac{\partial u_0}{\partial x} + \frac{1}{2}\left(\frac{\partial w_0}{\partial x}\right)^2\right] + A_{26}\left[\frac{1}{R}\frac{\partial v_0}{\partial \theta} + \frac{w_0}{R} + \frac{1}{2}\left(\frac{1}{R}\frac{\partial w_0}{\partial \theta}\right)^2\right] + A_{66}\left(\frac{1}{R}\frac{\partial u_0}{\partial \theta} + \frac{\partial v_0}{\partial x} + \frac{1}{R}\frac{\partial w_0}{\partial \theta}\frac{\partial w_0}{\partial x}\right)\right\} \frac{\ell}{2} \mathrm{d}\theta \mathrm{d}\xi \\
&= -\int_{-1}^{1}\int_{0}^{2\pi} g_{u_i}(\xi) t_{u_m}(\theta) \frac{\partial^2 u_0(x,\theta,t)}{\partial t^2} \rho h \frac{R\ell}{2} \mathrm{d}\theta \mathrm{d}\xi
\end{aligned} \tag{27}$$

$$\begin{aligned}
&\int_{-1}^{1}\int_{0}^{2\pi} g_{v_i}(\xi) \frac{\mathrm{d}t_{v_m}(\theta)}{\mathrm{d}\theta} \left(A_{12}\left[\frac{\partial u_0}{\partial x} + \frac{1}{2}\left(\frac{\partial w_0}{\partial x}\right)^2\right] + A_{22}\left[\frac{1}{R}\frac{\partial v_0}{\partial \theta} + \frac{w_0}{R} + \frac{1}{2}\left(\frac{1}{R}\frac{\partial w_0}{\partial \theta}\right)^2\right] + A_{26}\left(\frac{1}{R}\frac{\partial u_0}{\partial \theta} + \frac{\partial v_0}{\partial x} + \frac{1}{R}\frac{\partial w_0}{\partial \theta}\frac{\partial w_0}{\partial x}\right)\right) \frac{\ell}{2} \mathrm{d}\theta \mathrm{d}\xi + \\
&\int_{-1}^{1}\int_{0}^{2\pi} \frac{\mathrm{d}g_{v_i}(\xi)}{\mathrm{d}\xi} t_{v_m}(\theta) \left(A_{16}\left[\frac{\partial u_0}{\partial x} + \frac{1}{2}\left(\frac{\partial w_0}{\partial x}\right)^2\right] + A_{26}\left[\frac{1}{R}\frac{\partial v_0}{\partial \theta} + \frac{w_0}{R} + \frac{1}{2}\left(\frac{1}{R}\frac{\partial w_0}{\partial \theta}\right)^2\right] + A_{66}\left(\frac{1}{R}\frac{\partial u_0}{\partial \theta} + \frac{\partial v_0}{\partial x} + \frac{1}{R}\frac{\partial w_0}{\partial \theta}\frac{\partial w_0}{\partial x}\right)\right) R \mathrm{d}\theta \mathrm{d}\xi + \\
&\int_{-1}^{1}\int_{0}^{2\pi} g_{v_i}(\xi) \frac{\mathrm{d}t_{v_m}(\theta)}{\mathrm{d}\theta} \left(-\mathrm{d}_{21}\frac{\partial^{\mathrm{d}} w_0}{\partial x^2} + \mathrm{d}_{\mathrm{d}}\left(\frac{1}{R^2}\frac{\partial v_0}{\partial \theta} - \frac{1}{R^2}\frac{\partial^2 w_0}{\partial \theta^2}\right) + \mathrm{d}_{26}\left(\frac{1}{R}\frac{\partial v_0}{\partial x} - \frac{2}{R}\frac{\partial^2 w_0}{\partial x \partial \theta}\right)\right) \frac{1}{R}\frac{\ell}{2} \mathrm{d}\theta \mathrm{d}\xi + \\
&\int_{-1}^{1}\int_{0}^{2\pi} \frac{\mathrm{d}g_{v_i}(\xi)}{\mathrm{d}\xi} t_{v_m}(\theta) \left(-\mathrm{d}_{16}\frac{\partial^2 w_0}{\partial x^2} + \mathrm{d}_{26}\left(\frac{1}{R^2}\frac{\partial v_0}{\partial \theta} - \frac{1}{R^2}\frac{\partial^2 w_0}{\partial \theta^2}\right) + \mathrm{d}_{66}\left(\frac{1}{R}\frac{\partial v_0}{\partial x} - \frac{2}{R}\frac{\partial^2 w_0}{\partial x \partial \theta}\right)\right) \mathrm{d}\theta \mathrm{d}\xi + \\
&= -\int_{-1}^{1}\int_{0}^{2\pi} g_{v_i}(\xi) t_{v_m}(\theta) \frac{\partial^2 v_0(x,\theta,t)}{\partial t^2} \rho h \frac{R\ell}{2} \mathrm{d}\theta \mathrm{d}\xi,
\end{aligned} \tag{28}$$

Obviously, the stiffness terms A_{ij} and D_{ij} cannot be taken outside the integrals in VSCL shells. Using now Eq. (19), one arrives at an equation where the sole unknowns are generalised coordinates $\mathbf{q}_u$, $\mathbf{q}_v$ and $\mathbf{q}_w$. This will lead to the first two rows in the equation of motion, soon presented in abridged form using matrices and provided in detail in Appendix 1.

A similar procedure is applied to Eq. (26); the resulting equation is so large that it is not written in this subsection. Again, it is shortly given in abridged matrix form and its terms are expressed in detail in Appendix 1.

Terms from Piston Theory

According to piston theory, linear aerodynamics, the aerodynamic pressure, p_a, applied to the shell's surface as a consequence of external supersonic flow, $M>1.6$, can be written as [2]

$$p_a\left(x,\theta,t\right)=-\frac{\gamma p_\infty M^2}{\left(M^2-1\right)^{1/2}}\left[\frac{\partial w\left(x,\theta,t\right)}{\partial x}+\frac{1}{M\cdot a_\infty}\left(\frac{M^2-2}{M^2-1}\right)\frac{\partial w\left(x,\theta,t\right)}{\partial t}-\frac{w\left(x,\theta,t\right)}{2R(M^2-1)^{1/2}}\right] \tag{29}$$

where γ is the adiabatic exponent, p_∞ the freestream static pressure, a_∞ the freestream speed of sound and M the Mach number. Inserting $p_z(x,\theta,t)$ in the respective term of Eq. (26), one obtains three terms, two of the "aerodynamic stiffness type", one of the "aerodynamic damping type". These terms are, with the signs they will have in the final ordinary differential equations of motion, respectively as follows

$$R\frac{\gamma p_\infty M^2}{\left(M^2-1\right)^{1/2}}\int_{-1}^{1}f_{w_i}\left(\xi\right)\frac{\mathrm{d}f_{w_j}\left(\xi\right)}{\mathrm{d}\xi}\mathrm{d}\xi\int_0^{2\pi}t_{w_m}\left(\theta\right)t_{w_n}\left(\theta\right)\mathrm{d}\theta\,q_{w_{jn}}\left(t\right) \tag{30}$$

$$-\frac{\ell\gamma p_\infty}{4}\frac{M^2}{M^2-1}\int_{-1}^{1}f_{w_i}\left(\xi\right)f_{w_j}\left(\xi\right)\mathrm{d}\xi\int_0^{2\pi}t_{w_m}\left(\theta\right)t_{w_n}\left(\theta\right)\,\mathrm{d}\theta\,q_{w_{jn}}\left(t\right) \tag{31}$$

$$\frac{R\ell}{2}\frac{\gamma p_\infty}{a_\infty}\frac{M\left(M^2-2\right)}{\left(M^2-1\right)^{3/2}}\int_{-1}^{1}f_{w_i}\left(\xi\right)f_{w_j}\left(\xi\right)\mathrm{d}\xi\int_0^{2\pi}t_{w_m}\left(\theta\right)t_{w_n}\left(\theta\right)\mathrm{d}\theta\,\dot{q}_{w_{jn}}\left(t\right) \tag{32}$$

Full model equations of motion in matrix form

The ordinary differential equations of motion are presented in full in Appendix 1. Using matrices, they can be written as follows

$$\begin{bmatrix}\mathbf{M}_{uu}&\mathbf{0}&\mathbf{0}\\\mathbf{0}&\mathbf{M}_{vv}&\mathbf{0}\\\mathbf{0}&\mathbf{0}&\mathbf{M}_{ww}\end{bmatrix}\begin{Bmatrix}\ddot{\mathbf{q}}_u\left(t\right)\\\ddot{\mathbf{q}}_v\left(t\right)\\\ddot{\mathbf{q}}_w\left(t\right)\end{Bmatrix}+\begin{bmatrix}\mathbf{0}&\mathbf{0}&\mathbf{0}\\\mathbf{0}&\mathbf{0}&\mathbf{0}\\\mathbf{0}&\mathbf{0}&\mathbf{C}_{piston}\end{bmatrix}\begin{Bmatrix}\dot{\mathbf{q}}_u\left(t\right)\\\dot{\mathbf{q}}_v\left(t\right)\\\dot{\mathbf{q}}_w\left(t\right)\end{Bmatrix}+\begin{bmatrix}\mathbf{K}_{uu}&\mathbf{K}_{uv}&\mathbf{K}_{uw}\\\mathbf{K}_{vu}&\mathbf{K}_{vv}&\mathbf{K}_{vw}\\\mathbf{K}_{wu}&\mathbf{K}_{wv}&\mathbf{K}_{ww}\end{bmatrix}\begin{Bmatrix}\mathbf{q}_u\left(t\right)\\\mathbf{q}_v\left(t\right)\\\mathbf{q}_w\left(t\right)\end{Bmatrix}+$$
$$\begin{bmatrix}\mathbf{0}&\mathbf{0}&\mathbf{0}\\\mathbf{0}&\mathbf{0}&\mathbf{0}\\\mathbf{0}&\mathbf{0}&\mathbf{K}_{piston}\end{bmatrix}\begin{Bmatrix}\mathbf{q}_u\left(t\right)\\\mathbf{q}_v\left(t\right)\\\mathbf{q}_w\left(t\right)\end{Bmatrix}+\begin{bmatrix}\mathbf{0}&\mathbf{0}&\mathbf{K}_{uw}^{nl_1}\left(\mathbf{q}_w\left(t\right)\right)\\\mathbf{0}&\mathbf{0}&\mathbf{K}_{vw}^{nl_1}\left(\mathbf{q}_w\left(t\right)\right)\\\mathbf{K}_{wu}^{nl_1}\left(\mathbf{q}_w\left(t\right)\right)&\mathbf{K}_{wv}^{nl_1}\left(\mathbf{q}_w\left(t\right)\right)&\mathbf{K}_{ww}^{nl_1}\left(\mathbf{q}_w\left(t\right)\right)+\mathbf{K}_{ww}^{nl_2}\left(\mathbf{q}_w\left(t\right)\right)\end{bmatrix}\begin{Bmatrix}\mathbf{q}_u\left(t\right)\\\mathbf{q}_v\left(t\right)\\\mathbf{q}_w\left(t\right)\end{Bmatrix}=\begin{Bmatrix}\mathbf{0}\\\mathbf{0}\\\mathbf{0}\end{Bmatrix} \tag{33}$$

The consistent $\mathbf{M}_u$, $\mathbf{M}_v$ and $\mathbf{M}_w$, the constant stiffness matrices $\mathbf{K}_k$, k=*uu, uv, vu, v v* and *ww*, and the matrices due to the air-structure interaction, $\mathbf{C}_{piston}$ and $\mathbf{K}_{piston}$ are equal to the ones of reference [31]. Stiffness matrices $\mathbf{K}_k^{nl_1}\left(\mathbf{q}_w\left(t\right)\right)$, k=*uw*, *vw, wu, wv* and *ww*, are linear functions of generalised coordinates $\mathrm{q}_w(t)$, they lead to quadratic terms in Eq. (33) (as detailed in Eqs. (A1), (A2) and (A3), Appendix 1). Finally, stiffness matrix $\mathbf{K}_k^{nl_2}\left(\mathbf{q}_w\left(t\right)\right)$ is a quadratic function of $\mathbf{q}_w(t)$; multiplied by the generalised coordinates, it leads to cubic terms in the equations of motion (33), terms that can be found in full in Eq. (A3), Appendix 1.

Equations of Motion – reduced-order Models

Determining flutter conditions requires solving an eigenvalue problem. When many degrees of freedom are involved, this problem is often ill-conditioned, demanding high numerical precision in the computations. By neglecting membrane inertia, a reduced-order model that is unaffected by high-frequency membrane waves can be obtained. This significantly reduces ill-conditioning issues. Beyond improved numerical stability, reduced-order models also offer the advantage of lower computational cost, which is particularly beneficial in non-linear analyses.

Two reduced-order models are now introduced. These will later be compared with the full model in case studies and one of them will be employed in the non-linear analyses.

Reduced-order Model 1 – no Membrane Inertia

In the absence of tangential external forces, and if the membrane inertia and membrane damping are neglected, then the membrane displacements can be written as

$$\left\{ \begin{array}{c} \mathbf{q}_u\left(t\right) \\ \mathbf{q}_v\left(t\right) \end{array} \right\} = -\left[\begin{array}{cc} \mathbf{K}_{uu} & \mathbf{K}_{uv} \\ \mathbf{K}_{vu} & \mathbf{K}_{vv} \end{array} \right]^{-1} \left[\begin{array}{c} \mathbf{K}_{uw} + \mathbf{K}_{uw}^{nl_1}\left(\mathbf{q}_w\left(t\right)\right) \\ \mathbf{K}_{vw} + \mathbf{K}_{vw}^{nl_1}\left(\mathbf{q}_w\left(t\right)\right) \end{array} \right] \mathbf{q}_w\left(t\right), \tag{34}$$

and the number of degrees of freedom reduced to np_w, Eq. (21), which is the number of ordinary differential equations of motion in $\mathbf{q}_w(t)$:

$$\begin{aligned} &\mathbf{M}_{ww}\ddot{\mathbf{q}}_w\left(t\right) + \left[\mathbf{C}_{ww} + \mathbf{C}_{piston}\right]\dot{\mathbf{q}}_w\left(t\right) + \left[\mathbf{K}_{ww} + \mathbf{K}_{piston}\right]\mathbf{q}_w\left(t\right) + \left[\mathbf{K}_{ww}^{nl_1}\left(\mathbf{q}_w\left(t\right)\right) + \mathbf{K}_{ww}^{nl_2}\left(\mathbf{q}_w\left(t\right)\right)\right]\mathbf{q}_w\left(t\right) \\ &\quad - \left(\left[\begin{array}{cc} \mathbf{K}_{wu} & \mathbf{K}_{wv} \end{array} \right] \left[\begin{array}{cc} \mathbf{K}_{uu} & \mathbf{K}_{uv} \\ \mathbf{K}_{vu} & \mathbf{K}_{vv} \end{array} \right]^{-1} \left[\begin{array}{c} \mathbf{K}_{uw} + \mathbf{K}_{uw}^{nl_1}\left(\mathbf{q}_w\left(t\right)\right) \\ \mathbf{K}_{vw} + \mathbf{K}_{vw}^{nl_1}\left(\mathbf{q}_w\left(t\right)\right) \end{array} \right] \right) \mathbf{q}_w\left(t\right) \\ &\quad - \left(\left[\begin{array}{cc} \mathbf{K}_{wu}^{nl_1}\left(\mathbf{q}_w\left(t\right)\right) & \mathbf{K}_{wv}^{nl_1}\left(\mathbf{q}_w\left(t\right)\right) \end{array} \right] \left[\begin{array}{cc} \mathbf{K}_{uu} & \mathbf{K}_{uv} \\ \mathbf{K}_{vu} & \mathbf{K}_{vv} \end{array} \right]^{-1} \left[\begin{array}{c} \mathbf{K}_{uw} + \mathbf{K}_{uw}^{nl_1}\left(\mathbf{q}_w\left(t\right)\right) \\ \mathbf{K}_{vw} + \mathbf{K}_{vw}^{nl_1}\left(\mathbf{q}_w\left(t\right)\right) \end{array} \right] \right) \mathbf{q}_w\left(t\right) = \mathbf{0} \end{aligned} \tag{35}$$

Note that the membrane displacements and the corresponding stiffness were not neglected. This procedure has successfully been applied in plates and open shallow shells [48]. It has also been employed in circular cylindrical, closed, isotropic, and constant stiffness shells [2]. As shown in Appendix 2, this approach imposes restrictions in the number of circumferential waves in the modes that can be analysed. However, as also demonstrated later, this will not be an issue for the non-linear oscillations of interest in this work.

Matrix $\mathbf{C}_{ww}$ represent viscous type damping in the structure; it can be obtained by a linear combination of the linear mass and structural stiffness matrices, a Rayleigh-type damping [49], with two parameters, a_1 and a_2, that may be identified using experiments.

By aggregating matrices of the same type, for simplicity, the reduced-order equations of motion can be written as

$$\begin{aligned} &\mathbf{M}\ddot{\mathbf{q}}_w\left(t\right) + \left(a_1\mathbf{M} + a_2\mathbf{K}_\ell + \mathbf{C}_{piston}\right)\dot{\mathbf{q}}_w\left(t\right) + \mathbf{K}_{n\ell c1}^{c}\left(\mathbf{q}_w\left(t\right)\right)\mathbf{q}_w\left(t\right) + \\ &\quad + \mathbf{K}_{n\ell c1}^{\mathbf{q}}\left(\mathbf{q}_w\left(t\right)\right)\mathbf{q}_w\left(t\right) + \mathbf{K}_{piston}\,\mathbf{q}_w\left(t\right) + \mathbf{K}_{\ell c1}\,\mathbf{q}_w\left(t\right) = \mathbf{0} \end{aligned} \tag{36}$$

The new matrices introduced in reduced-order equation of motion (36) are:

- $\mathbf{K}_{n\ell c1}^{c}\left(\mathbf{q}_w\left(t\right)\right)$– the stiffness matrix that leads to cubic terms;
- $\mathbf{K}_{n\ell c1}^{q}\left(\mathbf{q}_w\left(t\right)\right)$ – the stiffness matrix that leads to quadratic terms;
- $\mathbf{K}_{\ell_{c1}}$ –constant stiffness matrix, which leads to linear terms.

The forms of these matrices can be deduced by comparing Eqs. (35) and (36).

In addition, the equations of motion were multiplied by the inverse of the mass matrix, yielding

$$\begin{aligned} &\ddot{\mathbf{q}}_w\left(t\right) + \left(a_1\mathbf{I} + a_2\mathbf{M}^{-1}\mathbf{K}_{\ell c1} + \mathbf{M}^{-1}\mathbf{C}_{piston}\right)\dot{\mathbf{q}}_w\left(t\right) + \mathbf{M}^{-1}\mathbf{K}_{n\ell c1}^{c}\left(\mathbf{q}_w\left(t\right)\right)\mathbf{q}_w\left(t\right) + \\ &\quad + \mathbf{M}^{-1}\mathbf{K}_{n\ell c1}^{q}\left(\mathbf{q}_w\left(t\right)\right)\mathbf{q}_w\left(t\right) + \mathbf{M}^{-1}\mathbf{K}_{piston}\,\mathbf{q}_w\left(t\right) + \mathbf{M}^{-1}\mathbf{K}_{\ell c1}\,\mathbf{q}_w\left(t\right) = \mathbf{0} \end{aligned} \tag{37}$$

One advantage of using (37) instead of (36) is that it allows for a routine designed for standard eigenvalue problems, rather than generalised ones. This approach proved to be less prone to ill-conditioning.

Reduced-order Model 2 – no Longitudinal Inertia

The numerical tests will show that neglecting the membrane inertia leads to significant errors in the computation of some natural frequencies of vibration. The reason is rather evident: in these modes of vibration, the circumferential and

transverse accelerations have similar magnitudes—this is not a plate or a shallow, open, shell. Therefore, a model in which only the longitudinal inertia is neglected is now proposed. In this case, the longitudinal displacements are

$$\mathbf{q}_u(t) = -\mathbf{K}_{uu}^{-1}\cdot\mathbf{K}_{uv}\cdot\mathbf{q}_v(t) - \mathbf{K}_{uu}^{-1}\cdot\mathbf{K}_{uw}\cdot\mathbf{q}_w(t) - \mathbf{K}_{uu}^{-1}\cdot\mathbf{K}_{uw}^{nl_1}(\mathbf{q}_w(t))\cdot\mathbf{q}_w(t) \tag{38}$$

The reduced equations of motion (reduced-order model 2) are

$$\begin{aligned}
&\begin{bmatrix}\mathbf{M}_{vv} & \mathbf{0}\\ \mathbf{0} & \mathbf{M}_{ww}\end{bmatrix}\begin{Bmatrix}\ddot{\mathbf{q}}_v(t)\\ \ddot{\mathbf{q}}_w(t)\end{Bmatrix} + \begin{bmatrix}\mathbf{C}_{vv} & \mathbf{0}\\ \mathbf{0} & \mathbf{C}_{ww}+\mathbf{C}_{piston}\end{bmatrix}\begin{Bmatrix}\dot{\mathbf{q}}_v(t)\\ \dot{\mathbf{q}}_w(t)\end{Bmatrix} + \begin{bmatrix}\mathbf{K}_{vv} & \mathbf{K}_{vw}\\ \mathbf{K}_{wv} & \mathbf{K}_{ww}\end{bmatrix}\begin{Bmatrix}\mathbf{q}_v(t)\\ \mathbf{q}_w(t)\end{Bmatrix}\\
&\quad - \begin{bmatrix}\mathbf{K}_{vu}\\ \mathbf{K}_{wu}\end{bmatrix}\cdot\mathbf{K}_{uu}^{-1}\cdot\begin{bmatrix}\mathbf{K}_{uv} & \mathbf{K}_{uw}\end{bmatrix}\begin{Bmatrix}\mathbf{q}_v(t)\\ \mathbf{q}_w(t)\end{Bmatrix} + \begin{bmatrix}\mathbf{0} & \mathbf{0}\\ \mathbf{0} & \mathbf{K}_{piston}\end{bmatrix}\begin{Bmatrix}\mathbf{q}_v(t)\\ \mathbf{q}_w(t)\end{Bmatrix}\\
&\quad - \begin{bmatrix}\mathbf{K}_{vu}\\ \mathbf{K}_{wu}\end{bmatrix}\cdot\mathbf{K}_{uu}^{-1}\cdot\mathbf{K}_{uw}^{nl_1}(\mathbf{q}_w(t))\cdot\mathbf{q}_w(t) - \begin{bmatrix}0\\ \mathbf{K}_{wu}^{nl_1}(\mathbf{q}_w(t))\cdot\mathbf{K}_{uu}^{-1}\cdot\begin{bmatrix}\mathbf{K}_{uv} & \mathbf{K}_{uw}\end{bmatrix}\begin{Bmatrix}\mathbf{q}_v(t)\\ \mathbf{q}_w(t)\end{Bmatrix}\end{bmatrix}\\
&+\begin{bmatrix}\mathbf{0} & \mathbf{K}_{vw}^{nl_1}(\mathbf{q}_w(t))\\ \mathbf{K}_{wv}^{nl_1}(\mathbf{q}_w(t)) & \mathbf{K}_{ww}^{nl_1}(\mathbf{q}_w(t))+\mathbf{K}_{ww}^{nl_2}(\mathbf{q}_w(t))\end{bmatrix}\begin{Bmatrix}\mathbf{q}_v(t)\\ \mathbf{q}_w(t)\end{Bmatrix} - \begin{bmatrix}0\\ \mathbf{K}_{wu}^{nl_1}(\mathbf{q}_w(t))\cdot\mathbf{K}_{uu}^{-1}\cdot\mathbf{K}_{uw}^{nl_1}(\mathbf{q}_w(t))\cdot\mathbf{q}_w(t)\end{bmatrix} = \begin{Bmatrix}\mathbf{0}\\ \mathbf{0}\end{Bmatrix}
\end{aligned} \tag{39}$$

and the number of degrees of freedom reduced to n_{c2}, Eq. (21).

As in the previous section, equations of motion (39) were multiplied by the inverse of the mass matrix.

Linear Aeroelastic Stability

To find the critical freestream pressures at which stability is lost, only the linear part of the equations of motion is used [1]. These second-order linear equations are transformed into first-order differential equations by introducing a vector of generalised velocities. Taking Eqs. (37) as an example, one has

$$\begin{Bmatrix}\dot{\mathbf{y}}_w(t)\\ \dot{\mathbf{q}}_w(t)\end{Bmatrix} + \begin{bmatrix}a_1\mathbf{I}+a_2\mathbf{M}^{-1}\mathbf{K}_\ell+\mathbf{M}^{-1}\mathbf{C}_{piston} & \mathbf{M}^{-1}\mathbf{K}_{piston}+\mathbf{M}^{-1}\mathbf{K}_\ell\\ -\mathbf{I} & \mathbf{0}\end{bmatrix}\begin{Bmatrix}\mathbf{y}_w(t)\\ \mathbf{q}_w(t)\end{Bmatrix} = \begin{Bmatrix}\mathbf{0}\\ \mathbf{0}\end{Bmatrix} \tag{40}$$

where $\mathbf{y}_w(t)$ represents generalised transverse velocities.

The solution of (40) has the form

$$\begin{Bmatrix}\mathbf{y}_w(t)\\ \mathbf{q}_w(t)\end{Bmatrix} = e^{\lambda t}\begin{Bmatrix}\mathbf{y}_w^e\\ \mathbf{q}_w^e\end{Bmatrix} \tag{41}$$

leading to

$$\begin{bmatrix}-a_1\mathbf{I}+-a_2\mathbf{M}^{-1}\mathbf{K}_\ell-\mathbf{M}^{-1}\mathbf{C}_{piston} & \mathbf{M}^{-1}\mathbf{K}_{piston}+\mathbf{M}^{-1}\mathbf{K}_\ell\\ -\mathbf{I} & \mathbf{0}\end{bmatrix}\begin{Bmatrix}\mathbf{y}_w^e\\ \mathbf{q}_w^e\end{Bmatrix} = \lambda\begin{Bmatrix}\mathbf{y}_w^e\\ \mathbf{q}_w^e\end{Bmatrix} \tag{42}$$

The eigenvalues, λ, and the eigenvectors come as complex conjugate pairs, so that by adding the complex conjugates the dynamic response only presents a real component. The real part of the eigenvalues may be related to damping, using the term 'damping' in an inclusive sense, as is common in aeroelasticity, where this so-called 'damping' can represent energy that is imparted to the structure, rather than dissipated. The solution is stable if $Re(\lambda)<0$ and unstable if $Re(\lambda)>0$. If the imaginary part is different from zero, it is related to the angular frequency of the oscillating movement. Specifically, a conjugate pair of eigenvalues may be written as

$$\lambda_j, \bar{\lambda}_j = -\zeta_j\omega_j \pm i\omega_j\sqrt{1-\zeta_j^2} \tag{43}$$

with ζ_j representing damping ratios and ω_j undamped frequencies of vibration; the overbar indicates the complex conjugate. Flutter occurs when the real component of at least one eigenvalue λ changes to a positive value and the imaginary component is not null. If $Re(\lambda)>0$ and if $Im(\lambda)=0$, the instability is not accompanied by oscillations, it is known as divergence [1].

Hopf Bifurcations and Non-linear Oscillations of VSCL Shells

The model presented in the previous sections was tested through comparisons with published cases; further details on these verifications are provided in Appendix 2. In this

section, the dynamics of cylindrical VSCL shells under a supersonic airflow are analysed.

The values of the various parameters of interest are introduced in SubSect. "Material and Geometric Properties". The validity of the reduced model used in the case studies is addressed in SubSect. "Convergence and model reduction: choice of model for LCOs analysis". A linear analysis is performed in the first part of SubSect. "Hopf Bifurcations and LCOs on thin VSCL Shells" to identify the critical conditions for the onset of flutter (Hopf bifurcations) and to select layups for the non-linear analysis. These oscillations are the focus of the second part of the same subsection.

Material and Geometric Properties

The material properties of the VSCL shells now considered are equal to the ones of the plates experimentally analysed in [50], as given in Table 1.

The dimensions of the VSCL shell are given in Table 2. The length and the radius result from rounding the values from the experimentally analysed shell of references [3, 4]. In these references, the shell has a length of 15.4 in (0.39116 m) and a radius of 8.00 in (0.2032 m). The thickness is 0.0040 in (0.0001016 m). The thickness of our VSCL shell is 0.00018 m, making it a very thin shell that is adequate for Kirchhoff–Love's hypothesis even in the presence of short wavelengths. This value corresponds to the average measured thickness of a single layer in the curvilinear fibre-reinforced plate from [50] and is very close to the 0.000181 m thickness of a single layer of the real shells in [16]. With the layers reported in references [16] and [50] for manufactured VSCLs, this choice provides the closest feasible approximation to the shell thickness in [3, 4] and this is the reason for choosing such a small value; the conclusions of the present study are expected to remain, on the overall, valid for other thicknesses, with consequent changes in the dynamics pressure values and eventual re-consideration of the model condensation to employ.

Table 1 Material properties of VSCL shells analysed in Sect. "Hopf Bifurcations and Non-linear Oscillations of VSCL Shells"

Property	Value and units
Longitudinal Young modulus, E_1	126.3 GPa
Transverse Young modulus, E_2	8.765 GPa
In-plane shear modulus, G_{12}	4.92 GPa
Poisson's ratio, υ_{12}	0.334
Mass density, ρ	1556.7 kg·m^{-3}

Table 2 Dimensions

Property	Value (m)
Length, ℓ	0.4
Radius, R	0.2
Thickness, h	0.00018

In the course of this work, several values for Θ_0 and Θ_1 were tested to define the fibre paths using Eq. (18). To restrict the analysis domain without limiting the relevance of its conclusions, the shell is made up of a single layer with a fibre angle of 0º at $x=0$—that is, oriented in the longitudinal direction—in all cases. This orientation can be justified by specific boundary conditions, such as a connection to another substructure with the same fibre angle. Θ_1 ranges from 0º to 50º, with the former value providing the reference constant stiffness shell and the latter leading to the shell where the fibres experience the highest curvature. Data for values larger than 50º are not included here due to the manufacturing curvature constraint. In fact, following [51], the curvature should not exceed 2.062 m^{-1}. With $\Theta_1=50$º a value of 1.745 m^{-1} is achieved for the reference fibre path. This is still manufacturable with automated tow placement without the laminate forming kinks due to excessive curvature, provided the tow width is limited (less than 9 mm wide). Thus, $\Theta_1=50$º represents the upper limit in the present analysis, a threshold.

Convergence and model reduction: choice of model for LCOs analysis

In this section, the number of degrees of freedom and the validity of the reduced-order model used in the non-linear studies are analysed. Further scrutiny of the reduced-order procedures is provided in Appendix 2, which includes comparisons with published work. The airflow parameters from [3, 4], Table 3, and Mach number, M, equal to 3, are employed both here and in the said appendix.

For this section's test case, the fibre orientation of the variable stiffness shell is defined by $\Theta_0=0$º, $\Theta_1=30$º.

To limit its scope, the non-linear analysis of the following section will focus on flutter modes for which membrane inertia (i.e., inertia related both to circumferential and longitudinal accelerations) is negligible. According to reference [2], page 38, this is feasible if the circumferential waves of the modes have a large number n, specifically, $n\geq 4$ or 5.

To verify if the former consideration applies to the VSCL shell that will be analysed, linear natural frequencies of a clamped–clamped shell are computed using the previously presented three models: the full model, the model neglecting longitudinal inertia, and the model neglecting membrane inertia (Table 4). Furthermore, to verify whether convergence has been achieved, results from models with seven, twelve and twenty unidimensional shape functions in ξ are compared, with the latter providing the reference

Table 3 Airflow parameters [3, 4]

Property	Value and units
Air's adiabatic exponent, γ	1.4
Air's speed of sound, a_∞	213.36 m/s

Table 4 Linear natural frequencies (rad/s) of CC VSCL shell, properties given in Tables 1, 2 and 3. Thirty circumferential functions. Full and reduced models [1,2]

	7 functions ofξ	12 functions ofξ			20 functions ofξ
#	Full model	Full model	Reduced model 1	Reduced model 2	Full model
1	1085.5	1080.6	1080.6	1083	1080.0
2	1088.6	1082.3	1082.3	1085.1	1081.7
3	1111.4	1107.5	1107.5	1109.7	1107.1
4	1124.4	1116.7	1116.7	1120	1115.8
5	1162	1159.1	1159.1	1161.1	1158.8
6	1196.1	1187.0	1187.0	1191.2	1186.0
7	1233.2	1231.1	1231.1	1233.0	1230.9
8	1307.3	1296.7	1296.7	1302.1	1295.6
9	1321.5	1319.9	1319.9	1321.8	1319.8
10	1423.8	1422.6	1422.6	1424.4	1422.5
11	1462.4	1450.5	1450.5	1457.7	1449.2
12	1537.7	1536.7	1536.7	1538.5	1536.6
13	1661.3	1655.7	1655.7	1662.3	1654.3
14	1669.1	1660.5	1660.5	1665.9	1660.5
15	1793.6	1792.9	1792.9	1794.6	1792.8
16	1830.2	1815.3	1815.3	1818.1	1814.4
17	1835.3	1822.9	1822.9	1825.5	1822.2
18	1857.0	1839.2	1839.2	1842.4	1838.2
19	1869.1	1859.0	1859.0	1861.4	1858.5
20	1918.4	1897.5	1897.5	1901.3	1896.4

1 – Longitudinal inertia neglected; 2 – membrane inertia neglected; # - mode number

values. Modes with more than thirty circumferential waves will not be considered throughout the paper and thirty functions in θ, for each of the three displacement components, were employed in this section. The circumferential functions are from Eqs. (22) and (23), starting with a constant ($t_{u_1}(\theta) = t_{v_1}(\theta) = t_{w_1}(\theta) = 1$).

Figures 2 and 3 complement Table 4 by showing the relative differences between natural frequency values obtained using the different models. Since higher-order modes can appear in flutter problems, and visual representations make it easier to interpret information, these figures even extend to higher-order modes than those included in the table.

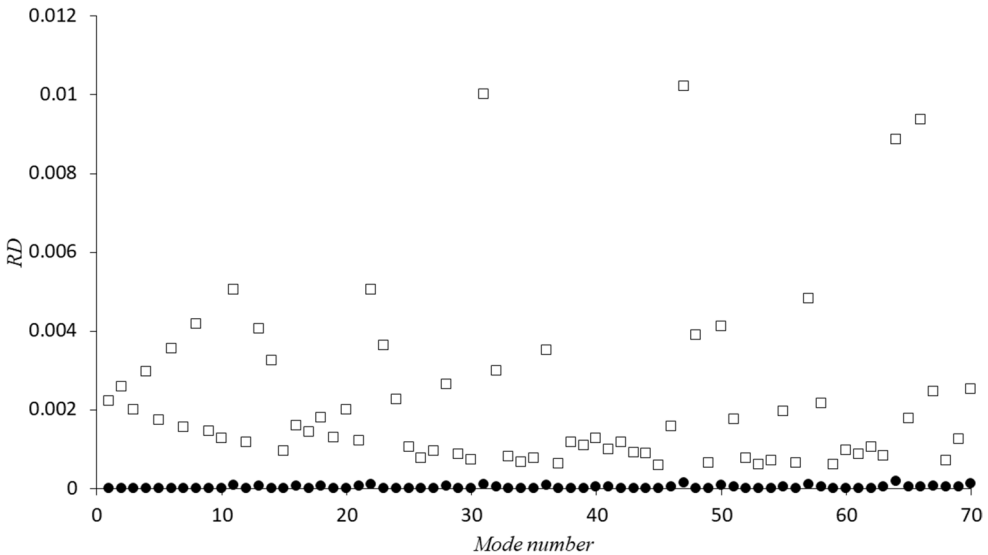

Fig. 2 Relative difference (*RD*) of natural frequencies computed using the full model and the models without: ● longitudinal inertia; □ membrane inertia. CC VSCL, properties in Tables 1 and 2. Each of the three displacement components is approached using thirty circumferential functions (θ) and twelve longitudinal functions (ξ)

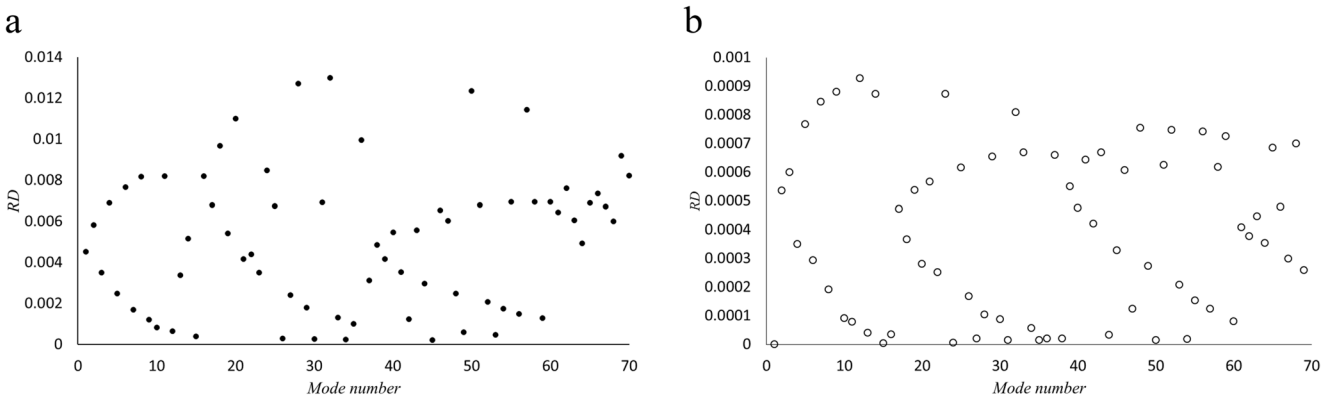

Fig. 3 Relative difference (*RD*) of natural frequencies computed using full models with: (**a**) 7 and 20 longitudinal functions (**b**) 12 and 20 longitudinal functions. CC VSCL, properties in Tables 1 and 2. Thirty circumferential functions (θ) are used for each of the three displacement components

Longitudinal inertia can be neglected without any error – at least up to the fifth significant digit – in the calculations performed. Membrane inertia can be neglected – at least until mode number 70 – with an error lower than 1.006% (Fig. 2). The full model with 7 functions of ξ per displacement component provides quite reasonable accuracy, with a relative difference of less than 1.4% compared to the full model with 20 functions in ξ, as shown in Fig. 3.

The last results of this subsection concern modes of vibration with circumferential waves of low wavenumber. Figure 4 gives the relative differences in the calculation of natural frequency of vibration values between a full model that does not contain these waves and one that does. Specifically, the former model resorts to 26 functions of θ, starting with functions that have four circumferential waves ($n=4$); the latter model employs 30 functions, starting with a constant function. In both cases, 7 functions of ξ per displacement component are employed. In this shell, circumferential waves with low values of n are only relevant for modes of vibration at or above mode number 183. This result is physically related to the low relevance of membrane inertia in this thin shell, since this inertia is more important when the number of circumferential waves is low (Appendix 2).

The analyses of this subsection indicate that both longitudinal and circumferential inertia (inertia related to accelerations $\ddot{u}$ and $\ddot{v}$) can be neglected in the analysis of the VSCL shell of interest. They also show that models using 7 functions of ξ provide accurate natural frequency values for a very large number of modes of vibration.

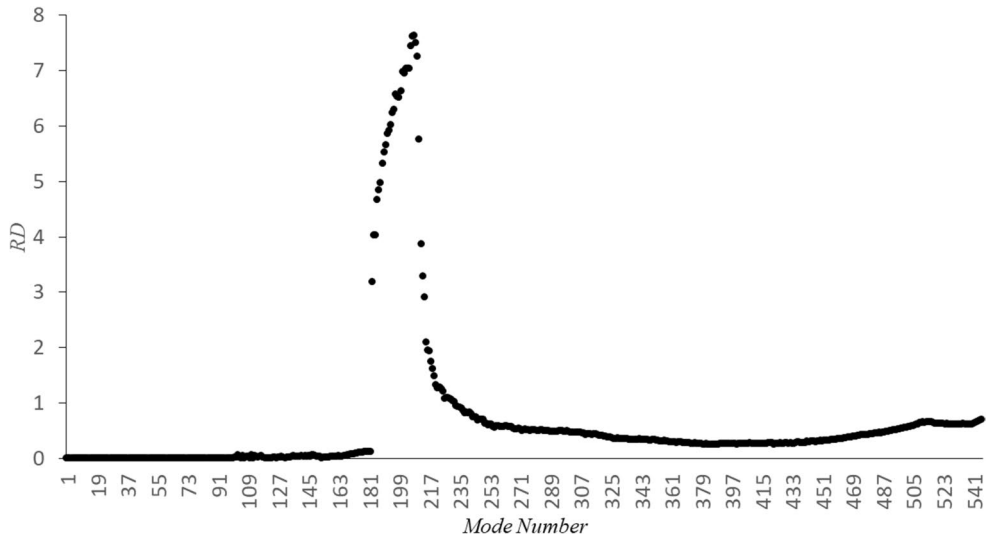

Fig. 4 Relative difference between full models with functions of θ ranging from 1 to 30 and from 4 to 30, Eqs. (22) and (23); 7 functions of ξ; CC VSCL thin circular cylindrical shell, properties in Tables 1 and 2

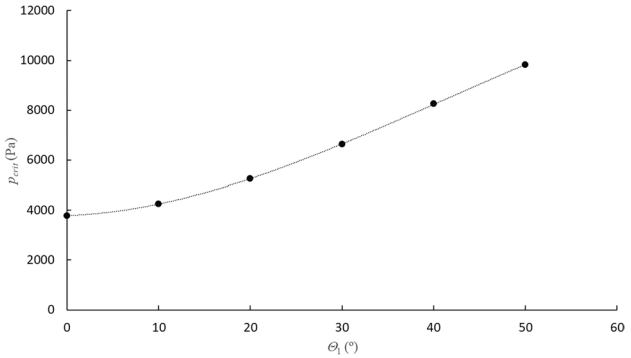

Fig. 5 Critical freestream pressure, p_{crit}, shells [$<0^o$, $\Theta_1>$]. Reduced model without membrane inertia. Shell clamped at both ends. $h=0.0018$ m, $R=0.2$, $\ell/R=2$. Twelve functions of ξ per displacement component; 26 functions of θ per displacement component. Starting number for circumferential functions: 4

Hopf Bifurcations and LCOs on thin VSCL Shells

Critical Freestream Pressure

Now, the values of the critical freestream pressures are determined for various VSCL shells clamped at both ends. The Mach number was set to 3.5; the remaining properties of interest are as given in Tables 2 and 3. The results presented in this subsection were computed using reduced models without membrane inertia, with twelve shape functions in ξ and thirty functions of θ, both per displacement component, as verified to be sufficient in the previous section.

In Fig. 5, the values of the critical freestream pressure, p_{crit}, for thin VSCL shells [$<0^o$, $\Theta_1>$] are represented as a function of Θ_1. Flutter occurred in all cases, not divergence.

Non-linear Oscillations

In this subsection, non-linear oscillations are analysed. The shells are identified by the respective values of Θ_1, since the fibre orientation at the left end, $x=0$, is equal in all shells. We start by addressing the variation of the oscillation amplitudes with: the fundamental frequencies of the respective oscillations (Fig. 6(a)); the freestream pressure (Fig. 6(b)).

Hardening spring effect is found in all cases. By slightly curving the fibre path, i.e., going from $\Theta_1=0^o$ to $\Theta_1=10^o$, gains above 10% are achieved in the relation between dynamic pressure and oscillation magnitude (specifically, the critical pressure increases from 3785.7 Pa to 4261.8 Pa). The differences decrease as the oscillation amplitude grows and the membrane effects stiffen the shells, with the shell with straight fibres approaching the shell with slightly curved fibres. The fundamental frequencies of the limit cycles of these two shells are also close, with shell $\Theta_1=10^o$ marginally experiencing more cycles per second.

On the other hand, using a fibre path that deviates more strongly from a rectilinear configuration, $\Theta_1=50^o$, large gains are achieved – considering that fewer cycles per second should delay fatigue issues – in what concerns the oscillation frequencies of the respective LCOs, which are reduced, and the pressures for similar amplitude vibrations, which are much larger, Fig. 6. It is also found that the fibre path with greater curvature manages to achieve stable LCOs for a quite larger pressure range than the other paths. For example, at 15 000 and 25 000 Pa, periodic oscillations were only obtained for VSCL shell $\Theta_1=50$ °. Hence, the apparent lack of points in the plots of the constant stiffness and $\Theta_1=10$ ° shells. The larger values of the freestream pressure lead to non-periodic oscillations in these two shells, as illustrated further down. We will later also see that the LCOs of shell $\Theta_1=50$ °, although stable, increasingly deviate from harmonic as the said pressure increases.

Both in shell $\Theta_1=0^o$ and in shell $\Theta_1=10^o$, the instability is related to a shape with 28 circumferential waves and, as Fig. 7 shows, the shapes assumed by a longitudinal cross section of the shells along an oscillation cycle are rather

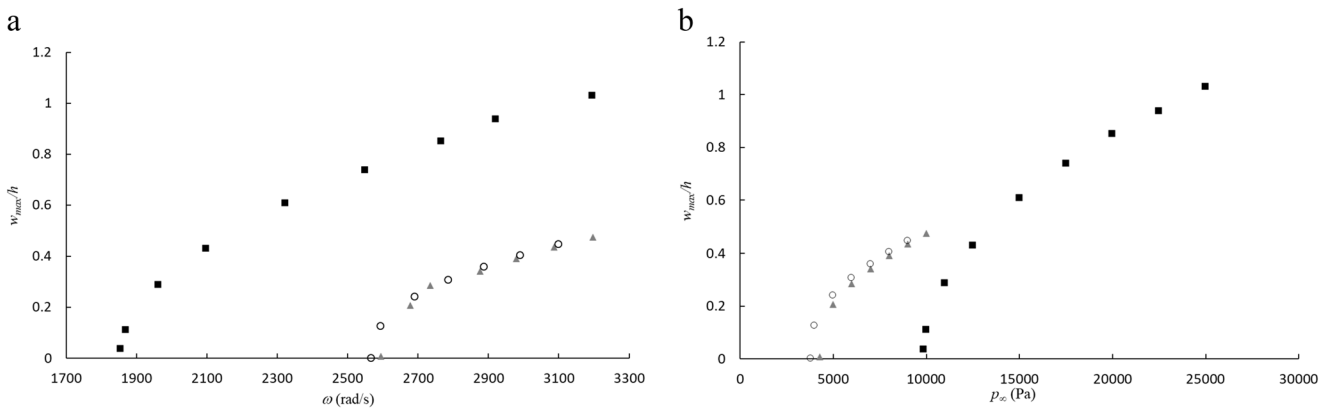

Fig. 6 (**a**) Non-dimensional amplitude at $(\xi, \theta)=(0.75, 0)$, versus oscillation frequency and (**b**) versus critical freestream pressure at $x=3\ell/4$, $\theta=0$: ○ $\Theta_1=0^o$; ▲ $\Theta_1=10^o$; ■ $\Theta_1=50^o$

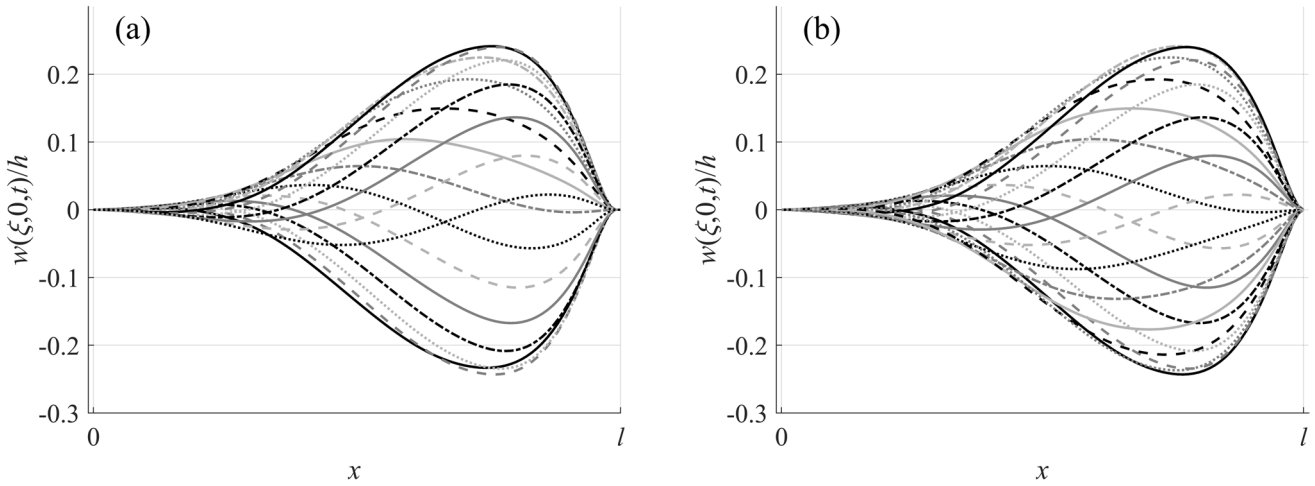

Fig. 7 Representation of deflection of a line on the cross section $\theta = 0$ of two shells (**a**) $\Theta_1 = 0^\circ$, (**b**) $\Theta_1 = 10^\circ$; different time instants along a cycle, $p_\infty = 5\,000$ Pa

similar. The part of each shell near the receiving end of the flow ($x = 0$) oscillates at much lower amplitudes than the other part.

Time histories and projections of the response in phase planes of the reference constant stiffness shell ($\Theta_1 = 0^\circ$), of the variable stiffness shell with lightly curved fibres ($\Theta_1 = 10^\circ$) and of the variable stiffness shell with strongly curved fibres ($\Theta_1 = 50^\circ$) are shown in Figs. 8 and 9. The corresponding values of the freestream static pressure are $p_\infty = 5\,000$ Pa and $p_\infty = 10\,000$ Pa. The plots correspond to point $x = 3\ell/4$, $\theta = 0$. Qualitatively similar plots were obtained in other points.

At $p_\infty = 5\,000$ Pa the variable stiffness shell $\Theta_1 = 50^\circ$ tends to its undeformed configuration, since this pressure is below its critical freestream pressure (Figs. 5 and 8). The other two shells undergo nearly harmonic limit cycle oscillations, with the constant stiffness shell experiencing larger magnitude oscillations. It is noteworthy that the shell that is stable is not the stiffer one (fundamental natural frequency of vibration equal to 1387 rad/s, $\Theta_1 = 50^\circ$), the contrary occurs, the stiffer shells (fundamental natural frequencies 2452 rad/s, $\Theta_1 = 0^\circ$, and 2645 rad/s, $\Theta_1 = 10^\circ$) are the ones that suffer Hopf bifurcations leading to LCOs. Flutter typically arises from mode coupling, so the larger stability domain observed for the $\Theta_1 = 50^\circ$ design is likely due to the increased separation between the interacting modes.

At $p_\infty = 10\,000$ Pa, the different fibre paths have even large consequences in the dynamics (Fig. 9). A periodic oscillation is not achieved by the constant stiffness shell. On the other hand, the VSCL where $\Theta_1 = 10^\circ$ experiences a stable LCO with oscillations of an amplitude that roughly corresponds to an average of the largest magnitude displacements achieved by the $\Theta_1 = 0^\circ$ shell. In VSCL shell $\Theta_1 = 50^\circ$, an LCO with an amplitude more than four times smaller than

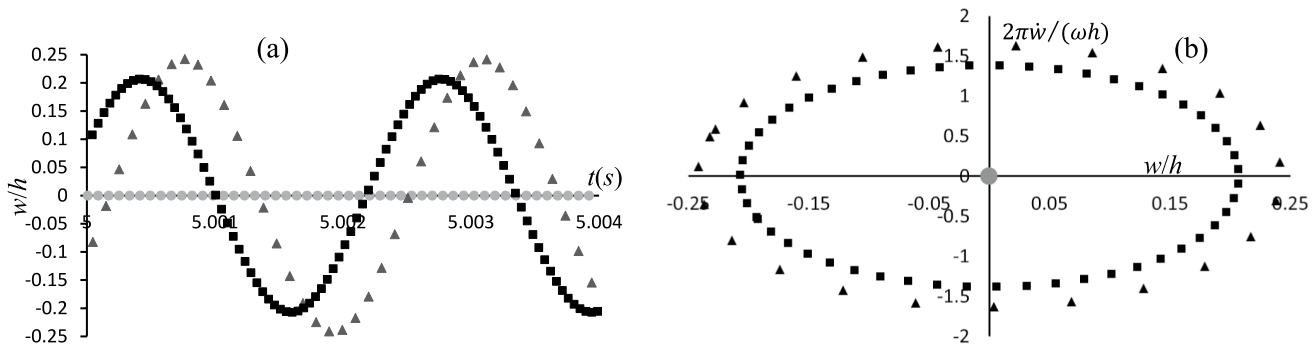

Fig. 8 (**a**) Time history and (**b**) projection on a phase plane of the steady-state response of the three shells when $p_\infty = 5\,000$ Pa, $x = 3\ell/4$, $\theta = 0$: ▲ $\Theta_1 = 0^\circ$, ■ $\Theta_1 = 10^\circ$, • $\Theta_1 = 50^\circ$

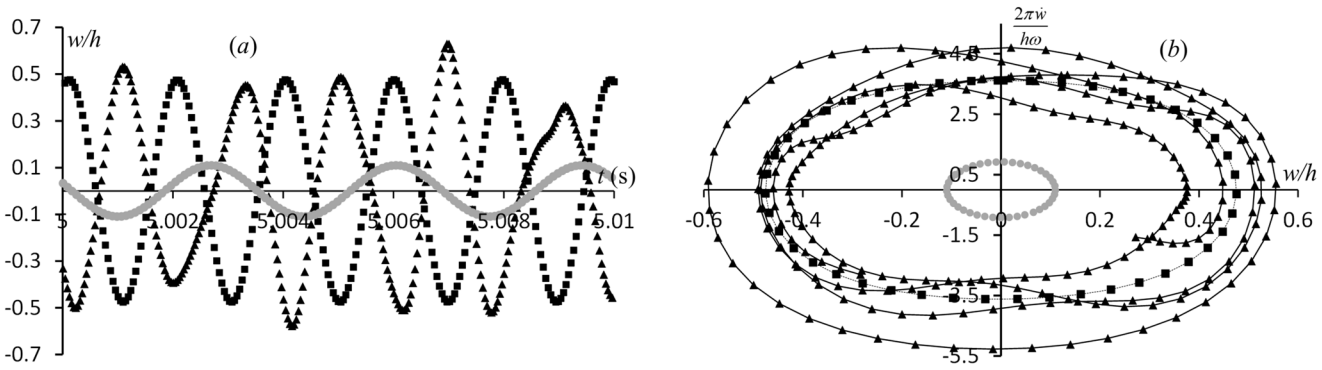

Fig. 9 (**a**) Time history and (**b**) projection on a phase plane of transverse oscillations of the three shells when $p_\infty = 10\,000$ Pa, point $x = 3\ell/4$, $\theta = 0$. ▲ $\Theta_1 = 0^o$, ■ $\Theta_1 = 10^o$, • $\Theta_1 = 50^o$. Lines were used in the phase plots

the one achieved by the variable stiffness composite shell $\Theta_1 = 10^o$ is attained. This example further demonstrates the large potential of curvilinear fibres in aeroelastic problems.

The time history of the transverse displacement of a point on the constant stiffness shell does not repeat (Fig. 9 (a), $\Theta_1 = 0^o$). In addition, the projection of the solution on a phase plane (Fig. 9(b), $\Theta_1 = 0^o$) does not lead to a close line, and its Fourier spectrum (Fig. 10) contains peaks at frequencies that are not commensurable, accompanied by a band of frequencies for which the response is "noise-like". These are features of an oscillation that is either quasi-periodic or chaotic [34].

To determine if the oscillation is chaotic or quasi-periodic, the largest Lyapunov exponent was computed using MatLab® function *lyapunovExponent*. The value estimated by this function changes with parameters *dim* and *lag* (respectively, the dimension of the space in which a phase portrait is reconstructed and the delay value used in phase space reconstruction [52]) employed in the algorithm and for that reason a value is not written here. Nonetheless, irrespective of the said parameters, a positive number - which corresponds to a chaotic oscillation - is consistently estimated. On the other hand, and to some extent verifying the validity of the MatLab® algorithm for Lyapunov exponent computation, when applied to isolated periodic oscillations, the same script regularly led to a largest Lyapunov exponent nearly equal to zero, as pertains to a stable limit cycle.

Shapes of a longitudinal cross section along the upper surface of the constant stiffness shell are shown in Fig. 11, for four values of the freestream pressure. Each plot presents various shapes at different times. Plots (a)-(c) are related to isolated closed trajectories on the phase space, i.e. to limit cycles, while plot (d) corresponds to chaotic oscillations. Travelling waves are patent in all cases, due to the phase differences in the oscillations of the diverse points.

As p_∞ increases from 5 000 Pa to 9 000 Pa (Figs. 7(a) and 11(a)-(c)), the shape corresponding to the maximum amplitude displacement becomes more evenly raised.

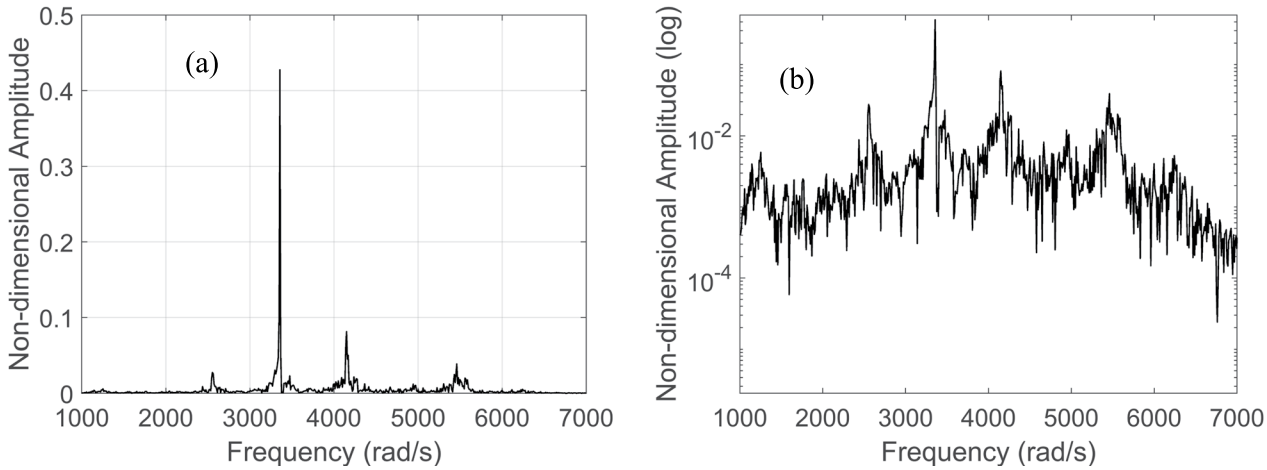

Fig. 10 FFT of transverse oscillation of constant stiffness shell when $p_\infty = 10\,000$ Pa, $x = 3\ell/4$, $\theta = 0^o$: (**a**) linear scale; (**b**) logarithmic scale

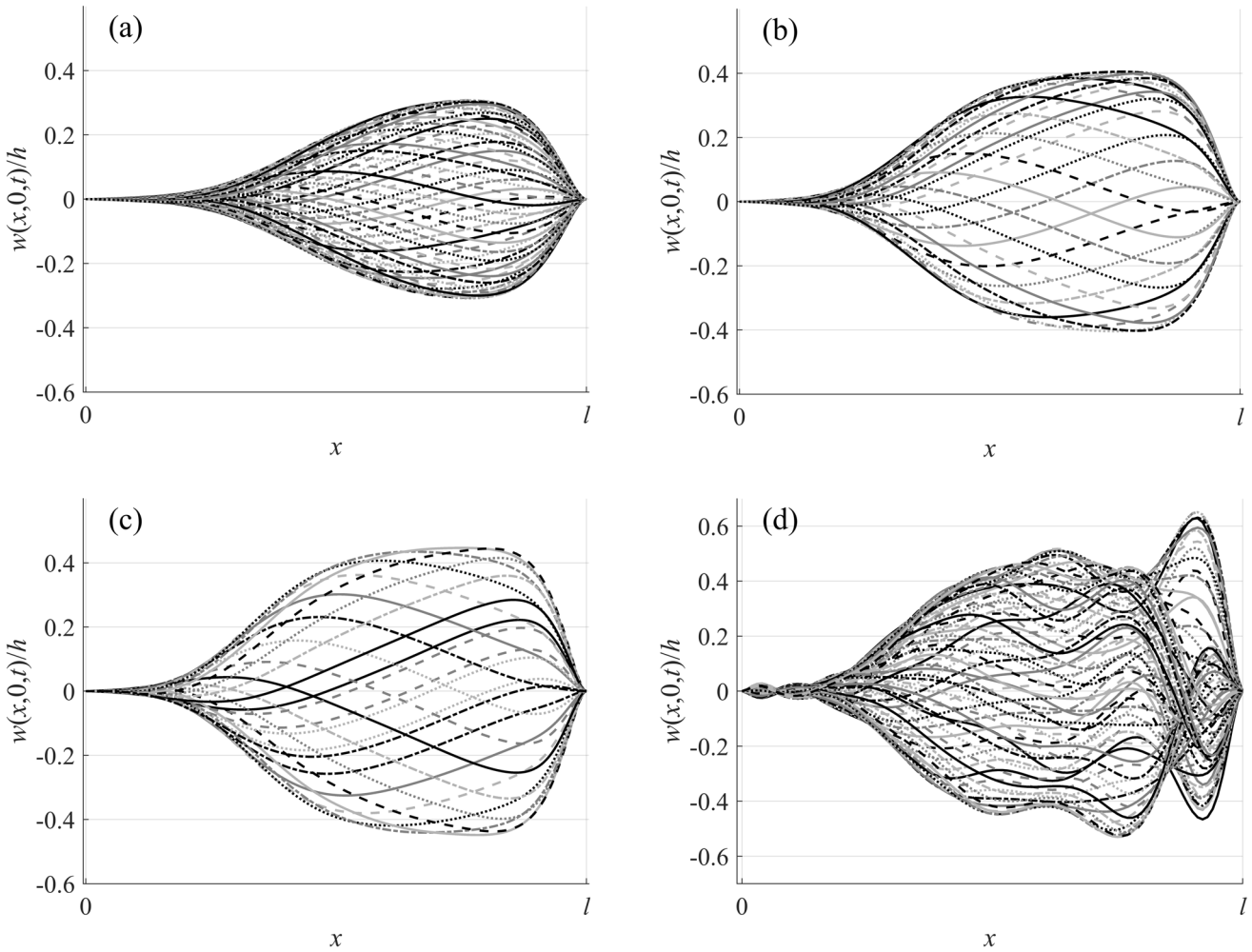

Fig. 11 Representation of deflection of a line on the cross section $\theta=0$ of shell $\Theta_0=0^o$, $\Theta_1=0^o$, different time instants at: (**a**) $p_\infty=6\,000$ Pa, (**b**) $p_\infty=8\,000$ Pa, (**c**) $p_\infty=9\,000$ Pa, (**d**) $p_\infty=10\,000$ Pa

Furthermore, the slope near the right clamped end increases, leading to larger curvatures and, therefore, to higher stresses. However, despite the pressure increase, the number of waves along the longitudinal direction remains small. In contrast, higher order structural modes are involved in the oscillations when chaos arises ($p_\infty=10\,000$ Pa), with the shell assuming much wavier shapes along the oscillation (Fig. 11 (d)).

To close this analysis, the examination of the dynamics of VSCL shell $\Theta_1=50$ º is continued. At larger freestream static pressures, as for example at 12 500 and 25 000 Pa, periodic oscillations still occur in this shell. Therefore, the projections of the solution on a phase plane are closed lines, Fig. 12. However, these oscillations are far from harmonic; hence, not only the trajectories in the phase plane deviate from ellipses but also symmetries with respect to the horizontal and vertical axes are lost. Correspondingly, the spectra of the responses at these larger freestream pressures distinctively show spikes at a fundamental frequency and some of its harmonics, Fig. 13. The magnitudes of the harmonics increase with the value of p_∞, as the periodic oscillations increasingly deviate from harmonic.

The longitudinal shape of shell $\Theta_1=50^o$ at low vibration amplitudes, shown in Fig. 14(a), displays travelling waves that do not differ significantly from those of shells $\Theta_1=0^o$ and $\Theta_1=10^o$ (Fig. 7) also at low vibration amplitudes. However, the shapes assumed by these LCOs in the shell $\Theta_1=50^o$ have 18 circumferential waves, instead of the 28 waves of the other shells. The lower number of circumferential waves mean that the corresponding curvatures (hence, the strains) are also lower for this shell.

At larger vibration amplitudes, longitudinal cross sections of shell $\Theta_1=50^o$ show a more even deflection of the shell, Fig. 14 (b). A similar change in shape also occurred in the other shells, but only shell $\Theta_1=50^o$ is able to maintain stable

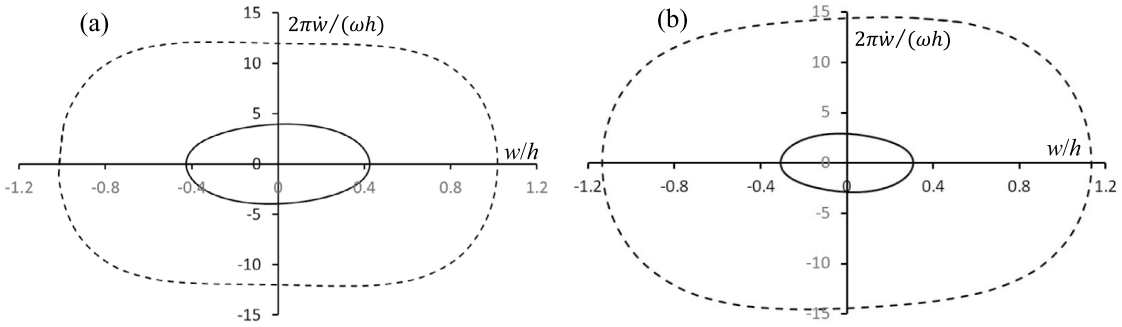

Fig. 12 Projection on a phase plane of LCOs of VSCL shell $\Theta_1 = 50^\circ$ when $p = 12\,500$ Pa — and $p = 25$---000 Pa—- -; points: $x = \ell/2$, $\theta = 0$ (**a**); $x = 3\ell/4$, $\theta = 0$ (**b**)

LCOs with this shape at significantly higher values of p_∞. This behaviour may be linked to the reduced stiffness near the right boundary caused by fibre inclination, which is consistent with the lower fundamental LCO frequencies observed for this shell. Being the oscillation frequencies lower, the aerodynamic power input is also likely to be lower, for the same freestream pressure, which would contribute to the enhanced stability of shell $\Theta_1 = 50^\circ$. Nonetheless, this hypothesis requires further analysis, since additional factors, as modal interactions and bifurcations, are likely to be involved.

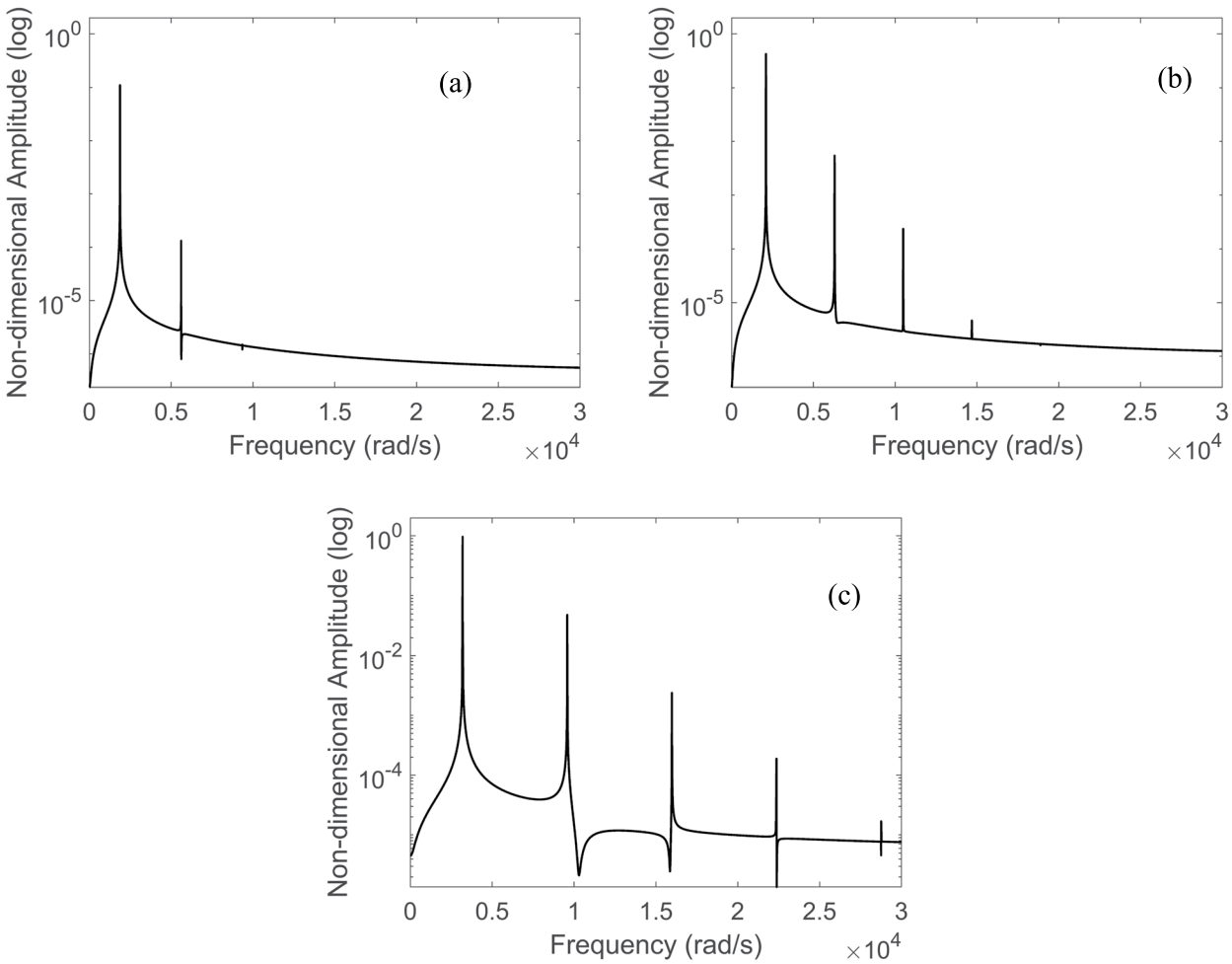

Fig. 13 FFT of transverse oscillation at $x = 3\ell/4$, $\theta = 0$, VSCL shell $\Theta_1 = 50^\circ$, when $p_\infty = 10\,000$ Pa (**a**), 12 500 (**b**) and 25 000 Pa (**c**)

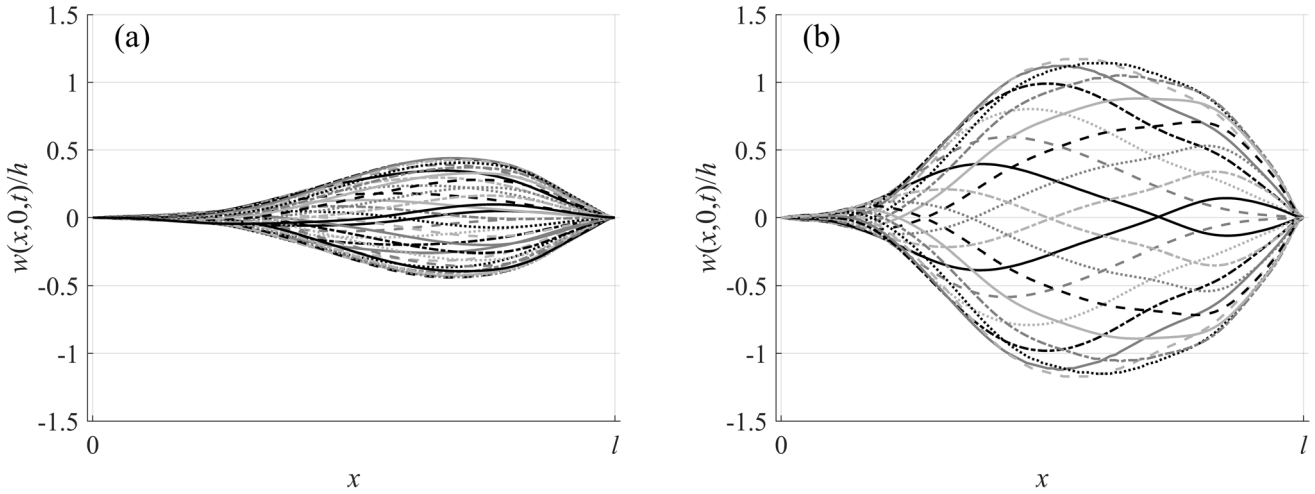

Fig. 14 Representation of deflection of a line on the cross section $\theta = 0$ of VSCL shell $\Theta_0 = 0^\circ$, $\Theta_1 = 50^\circ$, different time instants: (**a**) $p_\infty = 12\,500$ Pa, (**b**) $p_\infty = 25\,000$ Pa

Conclusion

Building on insights from a previous study in the linear regime, this research aimed to explore the effects of curvilinear fibres on large-amplitude oscillations in laminated cylindrical shells, with a focus on non-linear dynamics and model condensation. Theoretical and computational models were developed for thin, circular cylindrical shells made of laminated composite materials with curvilinear fibres, subjected to axial supersonic flows. Eigensolution routines were employed to find the natural frequencies and natural mode shapes of vibration, and to find the values of critical freestream pressure and the corresponding shapes. From these critical conditions, non-linear analyses were carried out, numerically solving the equations of motion in the time domain, hence obtaining nearly exact solutions.

It was confirmed that, also in this problem, neglecting the membrane inertia can lead to large errors in the computation of some natural frequencies of vibration. The reason is rather evident: in some modes of vibration, circumferential and transverse accelerations have similar orders of magnitude. On the other hand, it was shown that longitudinal inertia can still be neglected in these modes. It was also demonstrated that, for the very thin variable stiffness shell with fixed ends studied in the non-linear dynamic analyses, membrane inertia can be neglected without compromising accuracy over a very large frequency spectrum. Furthermore, it was verified that both reduced-order models mitigate ill-conditioning issues, in comparison to the full-order model.

A set of tests was carried out to assess whether using curvilinear reinforcing fibres instead of straight fibres offers advantages in non-linear oscillations after flutter. Both LCOs and non-periodic oscillations were found and characterised. Longitudinally travelling waves were described and it was shown that higher order modes are involved in chaotic oscillations. It was confirmed that curvilinear fibre paths can be employed to delay the onset of flutter, allowing for stable equilibrium configurations over a wider range of dynamic pressures than the reference straight-fibre configuration. More importantly, due to its novelty, the examinations performed in the non-linear regime demonstrate that curvilinear fibres also allow attaining LCOs with smaller amplitude displacements after flutter, permit to decrease the number of cycles per second and to increase the range for which the LCOs remain stable. The flutter onset delay is due to the separation of the frequencies of the intervening wind-off vibrations modes, the lower fundamental frequency of the limit cycles is likely a result of the smaller stiffness, near the right clamped end, of the VSCL shell modes involved in the oscillations. This enhanced behaviour may have positive reflections on fatigue life.

In addition to an, always desirable, experimental analysis, relevant future works include adding functions that are orthogonal to the ones considered in the circumferential approximation.

Appendix 1

Equations of Motion with All Terms Detailed

The equations of motion (33) are fully given in this appendix, row by row. Stiffness related terms are on the left hand side of the equations. The linear stiffness terms are written in black; the quadratic terms follow, grey. When cubic terms exist, they are written after the quadratic ones, again in black. Inertia terms and the term due to the aerodynamic force are on the right hand side.

The first line of Eqs. (33) is.

$$
\begin{aligned}
&\frac{2R}{\ell}\int_{-1}^{1}\frac{\mathrm{d}g_{u_i}(\xi)}{\mathrm{d}\xi}\frac{\mathrm{d}g_{u_j}(\xi)}{\mathrm{d}\xi}A_{11}(\xi)\mathrm{d}\xi\cdot\int_0^{2\pi}t_{u_m}(\theta)t_{u_n}(\theta)\mathrm{d}\theta\cdot q_{u_{jn}}(t)\\
&+\int_{-1}^{1}\frac{\mathrm{d}g_{u_i}(\xi)}{\mathrm{d}\xi}g_{v_j}(\xi)A_{12}(\xi)\mathrm{d}\xi\int_0^{2\pi}t_{u_m}(\theta)\frac{\mathrm{d}t_{u_n}(\theta)}{\mathrm{d}\theta}\mathrm{d}\theta\cdot q_{v_{jn}}(t)\ +\int_{-1}^{1}\frac{\mathrm{d}g_{u_i}(\xi)}{\mathrm{d}\xi}f_{w_j}(\xi)A_{12}(\xi)\mathrm{d}\xi\int_0^{2\pi}t_{u_m}(\theta)t_{w_n}(\theta)\mathrm{d}\theta\cdot q_{w_{jn}}(t)\\
&+\int_{-1}^{1}\frac{\mathrm{d}g_{u_i}(\xi)}{\mathrm{d}\xi}g_{u_j}(\xi)A_{16}(\xi)\mathrm{d}\xi\int_0^{2\pi}t_{u_m}(\theta)\frac{\mathrm{d}t_{u_n}(\theta)}{\mathrm{d}\theta}\mathrm{d}\theta\cdot q_{u_{jn}}(t)\\
&+\frac{2R}{\ell}\int_{-1}^{1}\frac{\mathrm{d}g_{u_i}(\xi)}{\mathrm{d}\xi}\frac{\mathrm{d}g_{v_j}(\xi)}{\mathrm{d}\xi}A_{16}(\xi)\mathrm{d}\xi\int_0^{2\pi}t_{u_m}(\theta)t_{v_n}(\theta)\mathrm{d}\theta\cdot q_{v_{jn}}(t)\\
&+\int_{-1}^{1}g_{u_i}(\xi)\frac{\mathrm{d}g_{u_j}}{\mathrm{d}\xi}(\xi)A_{16}(\xi)\mathrm{d}\xi\int_0^{2\pi}\frac{\mathrm{d}t_{u_m}(\theta)}{\mathrm{d}\theta}t_{u_n}(\theta)\mathrm{d}\theta q_{u_{jn}}(t)\\
&+\frac{\ell}{2R}\int_{-1}^{1}g_{u_i}(\xi)g_{v_j}(\xi)A_{26}(\xi)\mathrm{d}\xi\int_0^{2\pi}\frac{\mathrm{d}t_{u_m}(\theta)}{\mathrm{d}\theta}\frac{\mathrm{d}t_{v_n}(\theta)}{\mathrm{d}\theta}\mathrm{d}\theta q_{v_{jn}}(t)\\
&+\frac{\ell}{2R}\int_{-1}^{1}g_{u_i}(\xi)f_{w_j}(\xi)A_{26}(\xi)\mathrm{d}\xi\int_0^{2\pi}\frac{\mathrm{d}t_{u_m}(\theta)}{\mathrm{d}\theta}t_{w_n}(\theta)\mathrm{d}\theta q_{w_{jn}}(t)\\
&+\frac{\ell}{2R}\int_{-1}^{1}g_{u_i}(\xi)g_{u_j}(\xi)A_{66}(\xi)\mathrm{d}\xi\int_0^{2\pi}\frac{\mathrm{d}t_{u_m}(\theta)}{\mathrm{d}\theta}\frac{\mathrm{d}t_{u_n}(\theta)}{\mathrm{d}\theta}\mathrm{d}\theta\cdot q_{u_{jn}}(t)\\
&+\int_{-1}^{1}g_{u_i}(\xi)\frac{\mathrm{d}g_{v_j}(\xi)}{\mathrm{d}\xi}A_{66}(\xi)\mathrm{d}\xi\int_0^{2\pi}\frac{\mathrm{d}t_{u_m}(\theta)}{\mathrm{d}\theta}t_{v_n}(\theta)\mathrm{d}\theta q_{v_{jn}}(t)
\end{aligned}
$$

Quadratic terms

$$
\begin{aligned}
&+\frac{1}{2R}\int_{-1}^{1}\frac{\mathrm{d}g_{u_i}(\xi)}{\mathrm{d}\xi}f_{w_k}(\xi)f_{w_j}(\xi)A_{12}(\xi)\mathrm{d}\xi\int_0^{2\pi}t_{u_m}(\theta)\frac{\mathrm{d}t_{w_o}(\theta)}{\mathrm{d}\theta}\frac{\mathrm{d}t_{w_n}(\theta)}{\mathrm{d}\theta}\mathrm{d}\theta\cdot q_{w_{ko}}(t)q_{w_{jn}}(t)\\
&+\frac{2R}{\ell^2}\int_{-1}^{1}\frac{\mathrm{d}g_{u_i}(\xi)}{\mathrm{d}\xi}\frac{\mathrm{d}f_{w_k}(\xi)}{\mathrm{d}\xi}\frac{\mathrm{d}f_{w_j}(\xi)}{\mathrm{d}\xi}A_{11}(\xi)\mathrm{d}\xi\int_0^{2\pi}t_{u_m}(\theta)t_{w_o}(\theta)t_{w_n}(\theta)\mathrm{d}\theta\cdot q_{w_{ko}}(t)q_{w_{jn}}(t)\\
&+\frac{2}{\ell}\int_{-1}^{1}\frac{\mathrm{d}g_{u_i}(\xi)}{\mathrm{d}\xi}f_{w_k}(\xi)\frac{\mathrm{d}f_{w_j}(\xi)}{\mathrm{d}\xi}A_{16}(\xi)\mathrm{d}\xi\int_0^{2\pi}t_{u_m}(\theta)\frac{\mathrm{d}t_{w_o}(\theta)}{\mathrm{d}\xi}t_{w_n}(\theta)\mathrm{d}\theta q_{w_{ko}}(t)q_{w_{jn}}(t)\\
&+\frac{1}{\ell}\int_{-1}^{1}g_{u_i}(\xi)\frac{\mathrm{d}f_{w_k}(\xi)}{\mathrm{d}\xi}\frac{\mathrm{d}f_{w_j}(\xi)}{\mathrm{d}\xi}A_{16}(\xi)\mathrm{d}\xi\int_0^{2\pi}\frac{\mathrm{d}t_{u_m}}{\mathrm{d}\theta}t_{w_o}(\theta)t_{w_n}(\theta)\mathrm{d}\theta q_{w_{ko}}(t)q_{w_{jn}}(t)\\
&+\frac{\ell}{4R^2}\int_{-1}^{1}g_{u_i}(\xi)f_{w_k}(\xi)f_{w_j}(\xi)A_{26}(\xi)\mathrm{d}\xi\int_0^{2\pi}\frac{\mathrm{d}t_{u_m}(\theta)}{\mathrm{d}\theta}\frac{\mathrm{d}t_{w_o}(\theta)}{\mathrm{d}\theta}\frac{\mathrm{d}t_{w_n}(\theta)}{\mathrm{d}\theta}\mathrm{d}\theta q_{w_{ko}}(t)q_{w_{jn}}(t)\\
&+\frac{1}{R}\int_{-1}^{1}g_{u_i}(\xi)f_{w_k}(\xi)\frac{\mathrm{d}f_{w_j}(\xi)}{\mathrm{d}\xi}A_{66}(\xi)\mathrm{d}\xi\int_0^{2\pi}\frac{\mathrm{d}t_{u_m}(\theta)}{\mathrm{d}\theta}\frac{\mathrm{d}t_{u_o}(\theta)}{\mathrm{d}\theta}t_{w_n}(\theta)\mathrm{d}\theta q_{w_{ko}}(t)q_{w_{jn}}(t)
\end{aligned}
\tag{A1}
$$

$$
=-\rho h\frac{R\ell}{2}\int_{-1}^{1}g_{u_i}(\xi)g_{u_j}(\xi)\mathrm{d}\xi\int_{-1}^{1}\int_0^{2\pi}t_{u_m}(\theta)t_{u_n}(\theta)\mathrm{d}\theta\frac{\mathrm{d}^2q_{w_{jn}}(t)}{\mathrm{d}t^2}
$$

The second line of Eqs. (33) is, in detail, as follows.

$$
\int_{-1}^{1}g_{v_i}(\xi)A_{12}(\xi)\frac{\mathrm{d}g_{u_j}(\xi)}{\mathrm{d}\xi}\mathrm{d}\xi\int_0^{2\pi}\frac{\mathrm{d}t_{v_m}(\theta)}{\mathrm{d}\theta}t_{u_n}(\theta)\mathrm{d}\theta q_{u_{jn}}(t)+
$$

$$
\begin{aligned}
&+\frac{\ell}{2R}\int_{-1}^{1} g_{v_i}(\xi) A_{22}(\xi) g_{v_j}(\xi)\mathrm{d}\xi \int_0^{2\pi} \frac{\mathrm{d}t_{v_m}(\theta)}{\mathrm{d}\theta}\frac{\mathrm{d}t_{v_n}(\theta)}{\mathrm{d}\theta}\mathrm{d}\theta\, q_{v_{jn}}(t)+\\
&+\frac{\ell}{2R}\int_{-1}^{1} g_{v_i}(\xi) A_{22}(\xi) f_{w_j}(\xi)\mathrm{d}\xi \int_0^{2\pi} \frac{\mathrm{d}t_{v_m}(\theta)}{\mathrm{d}\theta} t_{w_n}(\theta)\mathrm{d}\theta\, q_{w_{jm}}(t)+\\
&+\frac{\ell}{2R}\int_{-1}^{1} g_{v_i}(\xi) g_{u_j}(\xi) A_{26}(\xi)\mathrm{d}\xi \int_0^{2\pi} \frac{\mathrm{d}t_{v_m}(\theta)}{\mathrm{d}\theta}\frac{\mathrm{d}t_{u_n}(\theta)}{\mathrm{d}\theta}\mathrm{d}\theta\, q_{u_{jm}}(t)+\\
&+\int_{-1}^{1} g_{v_i}(\xi)\frac{\mathrm{d}g_{v_j}(\xi)}{\mathrm{d}\xi} A_{26}(\xi)\mathrm{d}\xi \int_0^{2\pi} \frac{\mathrm{d}t_{v_m}(\theta)}{\mathrm{d}\theta} t_{v_n}(\theta)\mathrm{d}\theta\, q_{v_{jn}}(t)+\\
&2\frac{R}{\ell}\int_{-1}^{1} \frac{\mathrm{d}g_{v_i}(\xi)}{\mathrm{d}\xi}\frac{\mathrm{d}g_{u_j}(\xi)}{\mathrm{d}\xi} A_{16}(\xi)\mathrm{d}\xi \int_0^{2\pi} t_{v_m}(\theta) t_{u_n}(\theta)\mathrm{d}\theta\, q_{u_{jm}}(t)+\\
&\int_{-1}^{1} \frac{\mathrm{d}g_{v_i}(\xi)}{\mathrm{d}\xi} g_{v_j}(\xi) A_{26}(\xi)\mathrm{d}\xi \int_0^{2\pi} t_{v_m}(\theta)\frac{\mathrm{d}t_{v_n}(\theta)}{\mathrm{d}\theta}\mathrm{d}\theta\, q_{v_{jn}}(t)+\\
&\int_{-1}^{1} \frac{\mathrm{d}g_{v_i}(\xi)}{\mathrm{d}\xi} f_{w_j}(\xi) A_{26}(\xi)\mathrm{d}\xi \int_0^{2\pi} t_{v_m}(\theta) t_{w_n}(\theta)\mathrm{d}\theta\, q_{w_{jn}}(t)+\\
&\int_{-1}^{1} \frac{\mathrm{d}g_{v_i}(\xi)}{\mathrm{d}\xi} g_{u_j}(\xi) A_{66}(\xi)\mathrm{d}\xi \int_0^{2\pi} t_{v_m}(\theta)\frac{\mathrm{d}t_{u_n}(\theta)}{\mathrm{d}\theta}\mathrm{d}\theta\, q_{u_{jn}}(t)+\\
&\frac{2R}{\ell}\int_{-1}^{1} \frac{\mathrm{d}g_{v_i}(\xi)}{\mathrm{d}\xi}\frac{\mathrm{d}g_{v_j}(\xi)}{\mathrm{d}\xi} A_{66}(\xi)\mathrm{d}\xi \int_0^{2\pi} t_{v_m}(\theta) t_{v_n}(\theta)\mathrm{d}\theta\, q_{v_{jn}}(t)+\\
&+\frac{2}{R\ell}\int_{-1}^{1} \frac{\mathrm{d}g_{v_i}(\xi)}{\mathrm{d}\xi}\frac{\mathrm{d}f_{w_j}(\xi)}{\mathrm{d}\xi} D_{21}(\xi)\mathrm{d}\xi \int_0^{2\pi} \frac{\mathrm{d}t_{v_m}(\theta)}{\mathrm{d}\theta} t_{w_n}(\theta)\mathrm{d}\theta\, q_{w_{jn}}(t)+\\
&\frac{1}{R^3}\frac{\ell}{2}\int_{-1}^{1} g_{v_i}(\xi) g_{v_j}(\xi) D_{22}(\xi)\mathrm{d}\xi \int_0^{2\pi} \frac{\mathrm{d}t_{v_m}(\theta)}{\mathrm{d}\theta}\frac{\mathrm{d}t_{v_n}(\theta)}{\mathrm{d}\theta}\mathrm{d}\theta\, q_{v_{jn}}(t)+\\
&-\frac{1}{R^3}\frac{\ell}{2}\int_{-1}^{1} g_{v_i}(\xi) f_{w_j}(\xi) D_{22}(\xi)\mathrm{d}\xi \int_0^{2\pi} \frac{\mathrm{d}t_{v_m}(\theta)}{\mathrm{d}\theta}\frac{\mathrm{d}^2 t_{v_n}(\theta)}{\mathrm{d}\theta^2}\mathrm{d}\theta\, q_{w_{jn}}(t)\\
&\frac{1}{R^2}\int_{-1}^{1} g_{v_i}(\xi) D_{26}(\xi)\frac{\mathrm{d}g_{v_j}(\xi)}{\partial\xi}\mathrm{d}\xi \int_0^{2\pi} \frac{\mathrm{d}t_{v_m}(\theta)}{\mathrm{d}\theta} t_{v_n}(\theta)\mathrm{d}\theta\, q_{v_{jn}}(t)+\\
&-\frac{2}{R^2}\int_{-1}^{1} g_{v_i}(\xi) D_{26}(\xi)\frac{\mathrm{d}f_{w_j}(\xi)}{\partial\xi}\mathrm{d}\xi \int_0^{2\pi} \frac{\mathrm{d}t_{v_m}(\theta)}{\mathrm{d}\theta}\frac{\mathrm{d}t_{w_n}(\theta)}{\mathrm{d}\theta}\mathrm{d}\theta\, q_{w_{jn}}(t)+\\
&-\frac{4}{\ell^2}\int_{-1}^{1} \frac{\mathrm{d}g_{v_i}(\xi)}{\mathrm{d}\xi}\frac{\mathrm{d}^2 f_{w_j}(\xi)}{\mathrm{d}\xi^2} D_{16}(\xi)\mathrm{d}\xi \int_0^{2\pi} t_{v_m}(\theta) t_{w_n}(\theta)\mathrm{d}\theta\, q_{w_{jn}}(t)\\
&+\frac{1}{R^2}\int_{-1}^{1} D_{26}(\xi)\frac{\mathrm{d}g_{v_i}(\xi)}{\mathrm{d}\xi} g_{v_j}(\xi)\mathrm{d}\xi \int_0^{2\pi} t_{v_m}(\theta)\frac{\mathrm{d}t_{v_n}(\theta)}{\mathrm{d}\theta}\mathrm{d}\theta\, q_{v_{jn}}(t)\\
&+\frac{1}{R^2}\int_{-1}^{1} D_{26}(\xi)\frac{\mathrm{d}g_{v_i}(\xi)}{\mathrm{d}\xi} f_{w_j}(\xi)\mathrm{d}\xi \int_0^{2\pi} \frac{\mathrm{d}t_{v_m}(\theta)}{\mathrm{d}\theta}\frac{\mathrm{d}f_{w_n}(\theta)}{\mathrm{d}\theta}\mathrm{d}\theta\, q_{w_{jn}}(t)\\
&+\frac{2}{R\ell}\int_{-1}^{1} \frac{\mathrm{d}g_{v_i}(\xi)}{\mathrm{d}\xi}\frac{\mathrm{d}g_{v_j}(\xi)}{\mathrm{d}\xi} D_{66}(\xi)\mathrm{d}\xi \int_0^{2\pi} t_{v_m}(\theta) t_{v_n}(\theta)\mathrm{d}\theta\, q_{v_{jn}}(t)\\
&-\frac{4}{R\ell}\int_{-1}^{1} \frac{\mathrm{d}g_{v_i}(\xi)}{\mathrm{d}\xi}\frac{\mathrm{d}f_{w_j}(\xi)}{\mathrm{d}\xi} D_{66}(\xi)\mathrm{d}\xi \int_0^{2\pi} t_{v_m}(\theta)\frac{\mathrm{d}t_{w_n}(\theta)}{\mathrm{d}\theta}\mathrm{d}\theta\mathrm{d}\xi\, q_{w_{jn}}(t)+
\end{aligned}
\qquad \text{(A2)}
$$

Quadratic terms

$$
\begin{aligned}
&+\left(\frac{\ell}{4R^2}\int_{-1}^{1} g_{v_i}(\xi) f_{w_k}(\xi) f_{w_j}(\xi) A_{22}(\xi)\mathrm{d}\xi \int_0^{2\pi} \frac{\mathrm{d}t_{v_m}(\theta)}{\mathrm{d}\theta}\frac{\mathrm{d}t_{w_o}(\theta)}{\mathrm{d}\theta}\frac{\mathrm{d}t_{w_n}(\theta)}{\mathrm{d}\theta}\mathrm{d}\theta\, q_{w_{ko}}(t)\right) q_{w_{jn}}(t)+\\
&+\left(\frac{1}{\ell}\int_{-1}^{1} g_{v_i}(\xi)\frac{\mathrm{d}f_{w_k}(\xi)}{\mathrm{d}\xi}\frac{\mathrm{d}f_{w_j}(\xi)}{\mathrm{d}\xi} A_{22}(\xi)\mathrm{d}\xi \int_0^{2\pi} \frac{\mathrm{d}t_{v_m}(\theta)}{\mathrm{d}\theta} t_{w_o}(\theta) t_{w_n}(\theta)\mathrm{d}\theta\, q_{w_{ko}}(t)\right) q_{w_{jn}}(t)+\\
&+\left(\frac{1}{R}\int_{-1}^{1} g_{v_i}(\xi) f_{w_k}(\xi)\frac{\mathrm{d}f_{w_j}(\xi)}{\mathrm{d}\xi} A_{26}(\xi)\mathrm{d}\xi \int_0^{2\pi} \frac{\mathrm{d}t_{v_m}(\theta)}{\mathrm{d}\theta}\frac{\mathrm{d}t_{w_o}(\theta)}{\mathrm{d}\theta} t_{w_n}(\theta)\mathrm{d}\theta\, q_{w_{ko}}(t)\right) q_{w_{jn}}(t)+\\
&\left(2\frac{R}{\ell^2}\int_{-1}^{1} \frac{\mathrm{d}g_{v_i}(\xi)}{\mathrm{d}\xi}\frac{\mathrm{d}f_{w_k}(\xi)}{\mathrm{d}\xi}\frac{\mathrm{d}f_{w_j}(\xi)}{\mathrm{d}\xi} A_{16}(\xi)\mathrm{d}\xi \int_0^{2\pi} t_{v_m}(\theta) t_{u_o}(\theta) t_{u_n}(\theta)\mathrm{d}\theta\, q_{w_{ko}}(t)\right) q_{w_{jn}}(t)+\\
&\left(\frac{1}{2R}\int_{-1}^{1} \frac{\mathrm{d}g_{v_i}(\xi)}{\mathrm{d}\xi} f_{w_k}(\xi) f_{w_j}(\xi) A_{26}(\xi)\mathrm{d}\xi \int_0^{2\pi} t_{v_m}(\theta)\frac{\mathrm{d}t_{w_o}(\theta)}{\mathrm{d}\theta}\frac{\mathrm{d}t_{w_n}(\theta)}{\mathrm{d}\theta}\mathrm{d}\theta\, q_{w_{ko}}(t)\right) q_{w_{jn}}(t)+\\
&\left(\frac{2}{\ell}\int_{-1}^{1} \frac{\mathrm{d}g_{v_i}(\xi)}{\mathrm{d}\xi}\frac{\mathrm{d}f_{w_k}(\xi)}{\mathrm{d}\xi} f_{w_j}(\xi) A_{66}(\xi)\mathrm{d}\xi \int_0^{2\pi} t_{v_m}(\theta) t_{u_o}(\theta)\frac{\mathrm{d}t_{u_n}(\theta)}{\mathrm{d}\theta}\mathrm{d}\theta\, q_{w_{ko}}(t)\right) q_{w_{jn}}(t)+
\end{aligned}
$$

$$
= -\rho h\frac{R\ell}{2}\int_{-1}^{1} g_{v_i}(\xi) g_{v_j}(\xi)\mathrm{d}\xi \int_0^{2\pi} t_{v_m}(\theta) t_{v_n}(\theta)\mathrm{d}\theta\frac{\mathrm{d}^2 q_{v_{jn}}(t)}{\mathrm{d}t^2}
$$

Similarly, the third line of Eq. (33) is, with all terms detailed, as follows.

$$
\begin{aligned}
&-\int_{-1}^{1} f_{w_i}(\xi)\frac{\mathrm{d}g_{u_j}(\xi)}{\mathrm{d}\xi}A_{12}(\xi)\mathrm{d}\xi\int_0^{2\pi} t_{w_m}(\theta)t_{u_n}(\theta)\mathrm{d}\theta q_{u_{jn}}(t)\\
&-\frac{\ell}{2R}\int_{-1}^{1} f_{w_i}(\xi)A_{22}(\xi)g_{v_j}(\xi)\mathrm{d}\xi\int_0^{2\pi} t_{w_m}(\theta)\frac{\mathrm{d}t_{v_n}(\theta)}{\mathrm{d}\theta}\mathrm{d}\theta q_{v_{jn}}(t)\\
&-\frac{\ell}{2R}\int_{-1}^{1} f_{w_i}(\xi)A_{22}(\xi)f_{w_j}(\xi)\mathrm{d}\xi\int_0^{2\pi} t_{w_m}(\theta)t_{w_n}(\theta)\mathrm{d}\theta q_{w_{jn}}(t)\\
&-\frac{\ell}{2R}\int_{-1}^{1} f_{w_i}(\xi)g_{u_j}(\xi)A_{26}(\xi)\mathrm{d}\xi\int_0^{2\pi} t_{w_m}(\theta)\frac{\mathrm{d}t_{u_n}(\theta)}{\mathrm{d}\theta}\mathrm{d}\theta q_{u_{jn}}(t)\\
&-\int_{-1}^{1} f_{w_i}(\xi)\frac{\mathrm{d}g_{v_j}(\xi)}{\mathrm{d}\xi}A_{26}(\xi)\mathrm{d}\xi\int_0^{2\pi} t_{w_m}(\theta)t_{v_n}(\theta)\mathrm{d}\theta q_{v_{jn}}(t)\\
&-\frac{8R}{\ell^3}\int_{-1}^{1}\frac{\mathrm{d}^2 f_{w_i}(\xi)}{\mathrm{d}\xi^2}D_{11}\frac{\mathrm{d}^2 f_{w_j}(\xi)}{\mathrm{d}\xi^2}\mathrm{d}\xi\int_0^{2\pi} t_{w_m}(\theta)t_{w_n}(\theta)\mathrm{d}\theta q_{w_{jn}}(t)\\
&-\frac{2}{R\ell}\int_{-1}^{1}\frac{\mathrm{d}f_{w_i}(\xi)}{\mathrm{d}\xi}\frac{\mathrm{d}g_{v_j}(\xi)}{\mathrm{d}\xi}D_{12}(\xi)\mathrm{d}\xi\int_0^{2\pi} t_{w_m}(\theta)\frac{\mathrm{d}t_{v_n}(\theta)}{\mathrm{d}\theta}\mathrm{d}\theta q_{v_{jn}}(t)\\
&-\frac{2}{R\ell}\int_{-1}^{1}\frac{\mathrm{d}f_{w_i}(\xi)}{\mathrm{d}\xi}\frac{\mathrm{d}f_{w_j}(\xi)}{\mathrm{d}\xi}D_{12}(\xi)\mathrm{d}\xi\int_0^{2\pi}\frac{\mathrm{d}t_{w_m}(\theta)}{\mathrm{d}\theta}\frac{\mathrm{d}t_{w_n}(\theta)}{\mathrm{d}\theta}\mathrm{d}\theta q_{w_{jn}}(t)\\
&-\frac{4}{\ell^2}\int_{-1}^{1}\frac{\mathrm{d}f_{w_i}(\xi)}{\mathrm{d}\xi}\frac{\mathrm{d}^2 g_{v_j}(\xi)}{\mathrm{d}\xi^2}D_{16}(\xi)\mathrm{d}\xi\int_0^{2\pi} t_{w_m}(\theta)t_{v_n}(\theta)\mathrm{d}\theta q_{v_{jn}}(t)\\
&+\frac{8}{\ell^2}\int_{-1}^{1}\frac{\mathrm{d}f_{w_i}(\xi)}{\mathrm{d}\xi}\frac{\mathrm{d}^2 f_{w_j}(\xi)}{\mathrm{d}\xi^2}D_{16}(\xi)\mathrm{d}\xi\int_0^{2\pi} t_{w_m}(\theta)\frac{\mathrm{d}t_{w_n}(\theta)}{\mathrm{d}\theta}\mathrm{d}\theta q_{w_{jn}}(t)\\
&+\frac{4}{\ell^2}\int_{-1}^{1}\frac{\mathrm{d}f_{w_i}(\xi)}{\mathrm{d}\xi}\frac{\mathrm{d}^2 f_{w_j}(\xi)}{\mathrm{d}\xi^2}D_{16}(\xi)\mathrm{d}\xi\int_0^{2\pi} t_{w_m}(\theta)\frac{\mathrm{d}t_{w_n}(\theta)}{\mathrm{d}\theta}\mathrm{d}\theta q_{w_{jn}}(t)\\
&+\frac{1}{R^2}\int_{-1}^{1}\frac{\mathrm{d}f_{w_i}(\xi)}{\mathrm{d}\xi}g_{v_j}(\xi)D_{26}(\xi)\mathrm{d}\xi\int_0^{2\pi}\frac{\mathrm{d}t_{w_m}(\theta)}{\mathrm{d}\theta}\frac{\mathrm{d}t_{v_n}(\theta)}{\mathrm{d}\theta}\mathrm{d}\theta q_{v_{jn}}(t)\\
&-\frac{1}{R^2}\int_{-1}^{1}\frac{\mathrm{d}f_{w_i}(\xi)}{\mathrm{d}\xi}f_{w_j}(\xi)D_{26}(\xi)\mathrm{d}\xi\int_0^{2\pi}\frac{\mathrm{d}t_{w_m}(\theta)}{\mathrm{d}\theta}\frac{\mathrm{d}^2 t_{w_n}(\theta)}{\mathrm{d}\theta^2}\mathrm{d}\theta q_{w_{jn}}(t)\\
&-\frac{2}{R\ell}\int_{-1}^{1}\frac{\mathrm{d}f_{w_i}(\xi)}{\mathrm{d}\xi}\frac{\mathrm{d}g_{v_i}(\xi)}{\mathrm{d}\xi}D_{66}(\xi)\mathrm{d}\xi\int_0^{2\pi} t_{w_m}(\theta)\frac{\mathrm{d}t_{v_n}(\theta)}{\mathrm{d}\theta}\mathrm{d}\theta q_{v_{jn}}(t)
\end{aligned}
\tag{A3}
$$

$$-\frac{8}{R\ell}\int_{-1}^{1}\frac{\mathrm{d}f_{w_i}(\xi)}{\mathrm{d}\xi}\frac{\mathrm{d}f_{w_j}(\xi)}{\mathrm{d}\xi}D_{66}(\xi)\mathrm{d}\xi\int_0^{2\pi}\frac{\mathrm{d}t_{w_m}(\theta)}{\mathrm{d}\theta}\frac{\mathrm{d}t_{w_n}(\theta)}{\mathrm{d}\theta}\mathrm{d}\theta\, q_{w_{jn}}(t)$$

$$+\frac{4}{\ell^2}\int_{-1}^{1}\frac{\mathrm{d}f_{w_i}(\xi)}{\mathrm{d}\xi}\frac{\mathrm{d}^2f_{w_j}(\xi)}{\mathrm{d}\xi^2}D_{16}(\xi)\mathrm{d}\xi\int_0^{2\pi}t_{w_m}(\theta)\frac{\mathrm{d}t_{w_n}(\theta)}{\mathrm{d}\theta}\mathrm{d}\theta\, q_{w_{jn}}(t)+\frac{1}{R^2}\int_{-1}^{1}\frac{\mathrm{d}f_{w_i}(\xi)}{\mathrm{d}\xi}g_{v_j}(\xi)D_{26}(\xi)\mathrm{d}\xi\bullet$$

$$\bullet\int_0^{2\pi}\frac{\mathrm{d}t_{w_m}(\theta)}{\mathrm{d}\theta}\frac{\mathrm{d}t_{v_n}(\theta)}{\mathrm{d}\theta}\mathrm{d}\theta\, q_{v_{jn}}(t)-\frac{1}{R^2}\int_{-1}^{1}\frac{\mathrm{d}f_{w_i}(\xi)}{\mathrm{d}\xi}f_{w_j}(\xi)D_{26}(\xi)\mathrm{d}\xi\int_0^{2\pi}\frac{\mathrm{d}t_{w_m}(\theta)}{\mathrm{d}\theta}\frac{\mathrm{d}^2t_{w_n}(\theta)}{\mathrm{d}\theta^2}\mathrm{d}\theta\, q_{w_{jn}}(t)$$

$$+\frac{2}{R\ell}\int_{-1}^{1}\frac{\mathrm{d}f_{w_i}(\xi)}{\mathrm{d}\xi}\frac{\mathrm{d}g_{v_j}(\xi)}{\mathrm{d}\xi}D_{66}(\xi)\mathrm{d}\xi\int_0^{2\pi}\frac{\mathrm{d}t_{w_m}(\theta)}{\mathrm{d}\theta}t_{v_n}(\theta)\mathrm{d}\theta q_{v_{jn}}(t)$$

$$-\frac{2}{\ell R}\int_{-1}^{1}\frac{\mathrm{d}f_{w_i}(\xi)}{\mathrm{d}\xi}\frac{\mathrm{d}f_{w_j}(\xi)}{\mathrm{d}\xi}D_{21}(\xi)\mathrm{d}\xi\int_0^{2\pi}\frac{\mathrm{d}t_{w_m}(\theta)}{\mathrm{d}\theta}\frac{\mathrm{d}t_{w_n}(\theta)}{\mathrm{d}\theta}\mathrm{d}\theta q_{w_{jn}}(t)$$

$$-\frac{\ell}{2R^3}\int_{-1}^{1}f_{w_i}(\xi)g_{v_j}(\xi)D_{22}(\xi)\mathrm{d}\xi\int_0^{2\pi}\frac{\mathrm{d}t_{w_m}(\theta)}{\mathrm{d}\theta}\frac{\mathrm{d}^2t_{v_n}(\theta)}{\mathrm{d}\theta^2}\mathrm{d}\theta q_{v_{jn}}(t)$$

$$-\frac{\ell}{2R^3}\int_{-1}^{1}f_{w_i}(\xi)f_{w_j}(\xi)D_{22}(\xi)\mathrm{d}\xi\int_0^{2\pi}\frac{\mathrm{d}^2t_{w_m}(\theta)}{\mathrm{d}\theta^2}\frac{\mathrm{d}^2t_{w_n}(\theta)}{\mathrm{d}\theta^2}\mathrm{d}\theta q_{w_{jn}}(t)$$

$$-\frac{1}{R^2}\int_{-1}^{1}f_{w_i}(\xi)\frac{\mathrm{d}g_{v_i}(\xi)}{\mathrm{d}\xi}D_{26}(\xi)\mathrm{d}\xi\int_0^{2\pi}\frac{\mathrm{d}t_{w_m}(\theta)}{\mathrm{d}\theta}\frac{\mathrm{d}t_{v_n}(\theta)}{\mathrm{d}\theta}\mathrm{d}\theta q_{v_{in}}(t)$$

$$+\frac{2}{R^2}\int_{-1}^{1}f_{w_i}(\xi)\frac{\mathrm{d}f_{w_j}(\xi)}{\mathrm{d}\xi}D_{26}(\xi)\mathrm{d}\xi\int_0^{2\pi}\frac{\mathrm{d}t_{w_m}(\theta)}{\mathrm{d}\theta}\frac{\mathrm{d}^2t_{w_n}(\theta)}{\mathrm{d}\theta^2}\mathrm{d}\theta q_{w_{in}}(t)$$

Quadratic terms

$$-\frac{1}{\ell}\int_{-1}^{1}f_{w_i}(\xi)A_{12}(\xi)\frac{\mathrm{d}f_{w_k}(\xi)}{\mathrm{d}\xi}\frac{\mathrm{d}f_{w_j}(\xi)}{\mathrm{d}\xi}\mathrm{d}\xi\int_0^{2\pi}t_{w_m}(\theta)t_{w_o}(\theta)t_{w_n}(\theta)\mathrm{d}\theta q_{w_{ko}}(t)q_{w_{jn}}(t)$$

$$-\frac{\ell}{4R^2}\int_{-1}^{1}f_{w_i}(\xi)A_{22}(\xi)f_{w_k}(\xi)f_{w_j}(\xi)\mathrm{d}\xi\int_0^{2\pi}t_{w_m}(\theta)\frac{\mathrm{d}t_{w_o}(\theta)}{\mathrm{d}\theta}\frac{\mathrm{d}t_{w_n}(\theta)}{\mathrm{d}\theta}\mathrm{d}\theta q_{w_{ko}}(t)q_{w_{jn}}(t)$$

$$-\frac{1}{R}\int_{-1}^{1}f_{w_i}(\xi)A_{26}(\xi)\frac{\mathrm{d}f_{w_k}(\xi)}{\mathrm{d}\xi}f_{w_j}(\xi)\mathrm{d}\xi\int_0^{2\pi}t_{w_m}(\theta)t_{w_o}(\theta)\frac{\mathrm{d}t_{w_n}(\theta)}{\mathrm{d}\theta}\mathrm{d}\theta q_{w_{ko}}(t)q_{w_{jn}}(t)$$

$$-R\frac{4}{\ell^2}\int_{-1}^{1}A_{11}(\xi)\frac{\mathrm{d}f_{w_i}(\xi)}{\mathrm{d}\xi}\frac{\mathrm{d}f_{w_k}(\xi)}{\mathrm{d}\xi}\frac{\mathrm{d}g_{u_j}(\xi)}{\mathrm{d}\xi}\mathrm{d}\xi\int_0^{2\pi}t_{w_m}(\theta)t_{w_o}(\theta)t_{u_n}(\theta)\mathrm{d}\theta q_{w_{ko}}(t)q_{u_{jn}}(t)$$

$$-\frac{2}{\ell}\int_{-1}^{1}\frac{\mathrm{d}f_{w_i}(\xi)}{\mathrm{d}\xi}g_{v_j}(\xi)\frac{\mathrm{d}f_{w_k}(\xi)}{\mathrm{d}\xi}A_{12}(\xi)\mathrm{d}\xi\int_0^{2\pi}t_{w_m}(\theta)\frac{\mathrm{d}t_{v_n}(\theta)}{\mathrm{d}\theta}t_{w_o}(\theta)\mathrm{d}\theta q_{v_{jn}}(t)q_{w_{ko}}(t)$$

$$-\frac{2}{\ell}\int_{-1}^{1}\frac{\mathrm{d}f_{w_i}(\xi)}{\mathrm{d}\xi}f_{w_k}(\xi)\frac{\mathrm{d}f_{w_j}(\xi)}{\mathrm{d}\xi}A_{12}(\xi)\mathrm{d}\xi\int_0^{2\pi}t_{w_m}(\theta)t_{w_o}(\theta)t_{w_n}(\theta)\mathrm{d}\theta q_{w_{ko}}(t)q_{w_{jn}}(t)$$

$$-\frac{2}{\ell}\int_{-1}^{1}\frac{\mathrm{d}f_{w_i}(\xi)}{\mathrm{d}\xi}\frac{\mathrm{d}f_{w_k}(\xi)}{\mathrm{d}\xi}g_{u_j}(\xi)A_{16}(\xi)\mathrm{d}\xi\int_0^{2\pi}t_{w_m}(\theta)t_{w_o}(\theta)\frac{\mathrm{d}t_{u_n}(\theta)}{\mathrm{d}\theta}\mathrm{d}\theta q_{w_{ko}}(t)q_{u_{jn}}(t)$$

$$-R\frac{4}{\ell^2}\int_{-1}^{1}\frac{\mathrm{d}f_{w_i}(\xi)}{\mathrm{d}\xi}\frac{\mathrm{d}f_{w_k}(\xi)}{\mathrm{d}\xi}\frac{\mathrm{d}g_{v_j}(\xi)}{\mathrm{d}\xi}A_{16}(\xi)\mathrm{d}\xi\int_0^{2\pi}t_{w_m}(\theta)t_{w_o}(\theta)t_{v_n}(\theta)\mathrm{d}\theta q_{w_{ko}}(t)q_{v_{jn}}(t)$$

$$-\frac{2}{\ell}\int_{-1}^{1}\frac{\mathrm{d}f_{w_i}(\xi)}{\mathrm{d}\xi}f_{w_k}(\xi)A_{16}(\xi)\frac{\mathrm{d}g_{u_j}(\xi)}{\mathrm{d}\xi}\mathrm{d}\xi\int_0^{2\pi}t_{w_m}(\theta)\frac{\mathrm{d}t_{w_o}(\theta)}{\mathrm{d}\theta}t_{u_n}(\theta)\mathrm{d}\theta q_{w_{ko}}(t)q_{u_{jn}}(t)$$

$$-\frac{1}{R}\int_{-1}^{1}\frac{\mathrm{d}f_{w_i}(\xi)}{\mathrm{d}\xi}f_{w_k}(\xi)g_{v_j}(\xi)A_{26}(\xi)\mathrm{d}\xi\int_0^{2\pi}t_{w_m}(\theta)\frac{\mathrm{d}t_{w_o}(\theta)}{\mathrm{d}\theta}\frac{\mathrm{d}t_{v_n}(\theta)}{\mathrm{d}\theta}\mathrm{d}\theta q_{w_{ko}}(t)q_{v_{jn}}(t)$$

$$
\begin{aligned}
&-\frac{1}{R}\int_{-1}^{1}\frac{\mathrm{d}f_{w_i}(\xi)}{\mathrm{d}\xi}f_{w_k}(\xi)f_{w_j}(\xi)A_{26}(\xi)\mathrm{d}\xi\int_0^{2\pi}t_{w_m}(\theta)\frac{\mathrm{d}t_{w_o}(\theta)}{\mathrm{d}\theta}t_{w_n}(\theta)\mathrm{d}\theta q_{w_{ko}}(t)q_{w_{jn}}(t)\\
&-\frac{1}{R}\int_{-1}^{1}\frac{\mathrm{d}f_{w_i}(\xi)}{\mathrm{d}\xi}f_{w_k}(\xi)g_{u_j}(\xi)A_{66}(\xi)\mathrm{d}\xi\int_0^{2\pi}t_{w_m}(\theta)\frac{\mathrm{d}t_{w_o}(\theta)}{\mathrm{d}\theta}\frac{\mathrm{d}t_{u_n}(\theta)}{\mathrm{d}\theta}\mathrm{d}\theta q_{w_{ko}}(t)q_{u_{jn}}(t)\\
&-\frac{2}{\ell}\int_{-1}^{1}\frac{\mathrm{d}f_{w_i}(\xi)}{\mathrm{d}\xi}f_{w_k}(\xi)\frac{\mathrm{d}g_{v_j}(\xi)}{\mathrm{d}\xi}A_{66}(\xi)\mathrm{d}\xi\int_0^{2\pi}t_{w_m}(\theta)\frac{\mathrm{d}t_{w_o}(\theta)}{\mathrm{d}\theta}t_{v_n}(\theta)\mathrm{d}\theta q_{w_{ko}}(t)q_{v_{jn}}(t)\\
&-\frac{1}{R}\int_{-1}^{1}f_{w_i}(\xi)\frac{\mathrm{d}f_{w_k}(\xi)}{\mathrm{d}\xi}g_{v_j}(\xi)A_{26}(\xi)\mathrm{d}\xi\int_0^{2\pi}\frac{\mathrm{d}t_{w_m}(\theta)}{\mathrm{d}\theta}t_{w_o}(\theta)\frac{\mathrm{d}t_{v_n}(\theta)}{\mathrm{d}\theta}\mathrm{d}\theta q_{w_{ko}}(t)q_{v_{jn}}(t)\\
&-\frac{1}{R}\int_{-1}^{1}f_{w_i}(\xi)\frac{\mathrm{d}f_{w_k}(\xi)}{\mathrm{d}\xi}f_{w_j}(\xi)A_{26}(\xi)\mathrm{d}\xi\int_0^{2\pi}\frac{\mathrm{d}t_{w_m}(\theta)}{\mathrm{d}\theta}t_{w_o}(\theta)t_{w_n}(\theta)\mathrm{d}\theta q_{w_{ko}}(t)q_{w_{jn}}(t)\\
&-\frac{2}{\ell}\int_{-1}^{1}f_{w_j}(\xi)A_{16}(\xi)\frac{\mathrm{d}f_{w_k}(\xi)}{\mathrm{d}\xi}\frac{\mathrm{d}g_{u_j}(\xi)}{\mathrm{d}\xi}\mathrm{d}\xi\int_0^{2\pi}\frac{\mathrm{d}t_{w_m}(\theta)}{\mathrm{d}\theta}t_{w_o}(\theta)t_{u_n}(\theta)\mathrm{d}\theta q_{w_{ko}}(t)q_{u_{jn}}(t)\\
&-\frac{1}{R}\int_{-1}^{1}f_{w_i}(\xi)\frac{\mathrm{d}f_{w_k}(\xi)}{\mathrm{d}\xi}g_{u_j}(\xi)A_{66}(\xi)\mathrm{d}\xi\int_0^{2\pi}\frac{\mathrm{d}t_{w_m}(\theta)}{\mathrm{d}\theta}t_{w_o}(\theta)\frac{\mathrm{d}t_{u_n}(\theta)}{\mathrm{d}\theta}\mathrm{d}\theta q_{w_{ko}}(t)q_{u_{jn}}(t)\\
&-\frac{2}{\ell}\int_{-1}^{1}f_{w_i}(\xi)\frac{\mathrm{d}f_{w_k}(\xi)}{\mathrm{d}\xi}\frac{\mathrm{d}f_{v_j}(\xi)}{\mathrm{d}\xi}A_{66}(\xi)\mathrm{d}\xi\int_0^{2\pi}\frac{\mathrm{d}t_{w_m}(\theta)}{\mathrm{d}\theta}t_{w_o}(\theta)t_{v_n}(\theta)\mathrm{d}\theta q_{w_{ko}}(t)q_{v_{jn}}(t)\\
&-\frac{1}{R}\int_{-1}^{1}\int_0^{2\pi}f_{w_i}(\xi)A_{12}(\xi)f_{w_k}(\xi)\frac{\mathrm{d}g_{u_j}(\xi)}{\mathrm{d}\xi}\mathrm{d}\theta\mathrm{d}\xi\int_0^{2\pi}\frac{\mathrm{d}t_{w_m}(\theta)}{\mathrm{d}\theta}\frac{\mathrm{d}t_{w_o}(\theta)}{\mathrm{d}\theta}t_{u_n}(\theta)\mathrm{d}\theta q_{w_{ko}}(t)q_{u_{jn}}(t)\\
&-\frac{\ell}{2R^2}\int_{-1}^{1}f_{w_i}(\xi)g_{v_j}(\xi)f_{w_k}(\xi)A_{22}(\xi)\mathrm{d}\xi\int_0^{2\pi}\frac{\mathrm{d}t_{w_m}(\theta)}{\mathrm{d}\theta}\frac{\mathrm{d}t_{v_n}(\theta)}{\mathrm{d}\theta}\frac{\mathrm{d}t_{w_o}(\theta)}{\mathrm{d}\theta}\mathrm{d}\theta q_{w_{ko}}(t)q_{v_{jn}}(t)\\
&-\frac{\ell}{2R^2}\int_{-1}^{1}f_{w_i}(\xi)f_{w_k}(\xi)f_{w_j}(\xi)A_{22}(\xi)\mathrm{d}\xi\int_0^{2\pi}\frac{\mathrm{d}t_{w_m}(\theta)}{\mathrm{d}\theta}\frac{\mathrm{d}t_{w_o}(\theta)}{\mathrm{d}\theta}t_{w_n}(\theta)\mathrm{d}\theta q_{w_{ko}}(t)q_{w_{jn}}(t)\\
&-\frac{\ell}{2R^2}\int_{-1}^{1}f_{w_i}(\xi)f_{w_k}(\xi)g_{u_j}(\xi)A_{26}(\xi)\mathrm{d}\xi\int_0^{2\pi}\frac{\mathrm{d}t_{w_m}(\theta)}{\mathrm{d}\theta}\frac{\mathrm{d}t_{w_o}(\theta)}{\mathrm{d}\theta}\frac{\mathrm{d}t_{u_n}(\theta)}{\mathrm{d}\theta}\mathrm{d}\theta q_{w_{ko}}(t)q_{u_{jn}}(t)\\
&-\frac{1}{R}\int_{-1}^{1}f_{w_i}(\xi)f_{w_k}(\xi)\frac{\mathrm{d}g_{v_j}(\xi)}{\mathrm{d}\xi}A_{26}(\xi)\mathrm{d}\xi\int_0^{2\pi}\frac{\mathrm{d}t_{w_m}(\theta)}{\mathrm{d}\theta}\frac{\mathrm{d}t_{w_o}(\theta)}{\mathrm{d}\theta}t_{v_n}(\theta)\mathrm{d}\theta q_{w_{ko}}(t)q_{v_{jn}}(t)
\end{aligned}
$$

Cubic terms

$$
\begin{aligned}
&-R\frac{4}{\ell^3}\int_{-1}^{1}A_{11}(\xi)\frac{\mathrm{d}f_{w_i}(\xi)}{\mathrm{d}\xi}\frac{\mathrm{d}f_{w_k}(\xi)}{\mathrm{d}\xi}\frac{\mathrm{d}f_{w_l}(\xi)}{\mathrm{d}\xi}\frac{\mathrm{d}f_{w_j}(\xi)}{\mathrm{d}\xi}\mathrm{d}\xi\int_0^{2\pi}t_{w_m}(\theta)t_{w_o}(\theta)t_{w_p}(\theta)t_{w_n}(\theta)\mathrm{d}\theta q_{w_{ko}}(t)q_{w_{lp}}(t)q_{w_{jn}}(t)\\
&-\frac{1}{\ell R}\int_{-1}^{1}\frac{\mathrm{d}f_{w_i}(\xi)}{\mathrm{d}\xi}f_{w_k}(\xi)\frac{\mathrm{d}f_{w_l}(\xi)}{\mathrm{d}\xi}f_{w_j}(\xi)A_{12}(\xi)\mathrm{d}\xi\int_0^{2\pi}t_{w_m}(\theta)\frac{\mathrm{d}t_{w_o}(\theta)}{\mathrm{d}\theta}t_{w_p}(\theta)\frac{\mathrm{d}t_{w_n}(\theta)}{\mathrm{d}\theta}\mathrm{d}\theta q_{w_{ko}}(t)q_{w_{lp}}(t)q_{w_{jn}}(t)\\
&-\frac{4}{\ell^2}\int_{-1}^{1}\frac{\mathrm{d}f_{w_i}(\xi)}{\mathrm{d}\xi}\frac{\mathrm{d}f_{w_k}(\xi)}{\mathrm{d}\xi}\frac{\mathrm{d}f_{w_l}(\xi)}{\mathrm{d}\xi}f_{w_j}(\xi)A_{16}(\xi)\mathrm{d}\xi\int_0^{2\pi}t_{w_m}(\theta)t_{w_o}(\theta)t_{w_p}(\theta)\frac{\mathrm{d}t_{w_n}(\theta)}{\mathrm{d}\theta}\mathrm{d}\theta q_{w_{ko}}(t)q_{w_{lp}}(t)q_{w_{jn}}(t)\\
&-\frac{2}{\ell^2}\int_{-1}^{1}\frac{\mathrm{d}f_{w_i}(\xi)}{\mathrm{d}\xi}f_{w_k}(\xi)\frac{\mathrm{d}f_{w_l}(\xi)}{\mathrm{d}\xi}\frac{\mathrm{d}f_{w_j}(\xi)}{\mathrm{d}\xi}A_{16}(\xi)\mathrm{d}\xi\int_0^{2\pi}t_{w_m}(\theta)\frac{\mathrm{d}t_{w_o}(\theta)}{\mathrm{d}\theta}t_{w_p}(\theta)t_{w_n}(\theta)\mathrm{d}\theta q_{w_{ko}}(t)q_{w_{lp}}(t)q_{w_{jn}}(t)\\
&-\frac{1}{2R^2}\int_{-1}^{1}\frac{\mathrm{d}f_{w_i}(\xi)}{\mathrm{d}\xi}f_{w_k}(\xi)f_{w_l}(\xi)f_{w_j}(\xi)A_{26}(\xi)\mathrm{d}\xi\int_0^{2\pi}t_{w_m}(\theta)\frac{\mathrm{d}t_{w_o}(\theta)}{\mathrm{d}\theta}\frac{\mathrm{d}t_{w_p}(\theta)}{\mathrm{d}\theta}\frac{\mathrm{d}t_{w_n}(\theta)}{\mathrm{d}\theta}\mathrm{d}\theta q_{w_{ko}}(t)q_{w_{lp}}(t)q_{w_{jn}}(t)\\
&-\frac{2}{R\ell}\int_{-1}^{1}\frac{\mathrm{d}f_{w_i}(\xi)}{\mathrm{d}\xi}f_{w_k}(\xi)f_{w_l}(\xi)\frac{\mathrm{d}f_{w_j}(\xi)}{\mathrm{d}\xi}A_{66}(\xi)\mathrm{d}\xi\int_0^{2\pi}t_{w_m}(\theta)\frac{\mathrm{d}t_{w_o}(\theta)}{\mathrm{d}\theta}\frac{\mathrm{d}t_{w_p}(\theta)}{\mathrm{d}\theta}t_{w_n}(\theta)\mathrm{d}\theta q_{w_{ko}}(t)q_{w_{lp}}(t)q_{w_{jn}}(t)\\
&-\frac{2}{\ell^2}\int_{-1}^{1}f_{w_i}(\xi)A_{16}(\xi)\frac{\mathrm{d}f_{w_k}(\xi)}{\mathrm{d}\xi}\frac{\mathrm{d}f_{w_l}(\xi)}{\mathrm{d}\xi}\frac{\mathrm{d}f_{w_j}(\xi)}{\mathrm{d}\xi}\mathrm{d}\xi\int_0^{2\pi}\frac{\mathrm{d}t_{w_m}(\theta)}{\mathrm{d}\theta}t_{w_o}(\theta)t_{w_p}(\theta)t_{w_n}(\theta)\mathrm{d}\theta q_{w_{ko}}(t)q_{w_{lp}}(t)q_{w_{jn}}(t)\\
&-\frac{1}{2}\frac{1}{R^2}\int_{-1}^{1}f_{w_i}(\xi)\frac{\mathrm{d}f_{w_k}(\xi)}{\mathrm{d}\xi}f_{w_l}(\xi)f_{w_j}(\xi)A_{26}(\xi)\mathrm{d}\xi\int_0^{2\pi}\frac{\mathrm{d}t_{w_m}(\theta)}{\mathrm{d}\theta}t_{w_o}(\theta)\frac{\mathrm{d}t_{w_p}(\theta)}{\mathrm{d}\theta}\frac{\mathrm{d}t_{w_n}(\theta)}{\mathrm{d}\theta}\mathrm{d}\theta q_{w_{ko}}(t)q_{w_{lp}}(t)q_{w_{jn}}(t)\\
&-\frac{2}{\ell R}\int_{-1}^{1}f_{w_i}(\xi)\frac{\mathrm{d}f_{w_k}(\xi)}{\mathrm{d}\xi}f_{w_l}(\xi)\frac{\mathrm{d}f_{w_j}(\xi)}{\mathrm{d}\xi}A_{66}(\xi)\mathrm{d}\xi\int_0^{2\pi}\frac{\mathrm{d}t_{w_m}(\theta)}{\mathrm{d}\theta}t_{w_o}(\theta)\frac{\mathrm{d}t_{w_p}(\theta)}{\mathrm{d}\theta}t_{w_n}(\theta)\mathrm{d}\theta q_{w_{ko}}(t)q_{w_{lp}}(t)q_{w_{jn}}(t)\\
&-\frac{1}{R\ell}\int_{-1}^{1}A_{12}(\xi)f_{w_i}(\xi)\frac{\mathrm{d}f_{w_k}(\xi)}{\mathrm{d}\xi}\frac{\mathrm{d}f_{w_l}(\xi)}{\mathrm{d}\xi}f_{w_j}(\xi)\mathrm{d}\xi\int_0^{2\pi}\frac{\mathrm{d}t_{w_m}(\theta)}{\mathrm{d}\theta}t_{w_o}(\theta)t_{w_p}(\theta)\frac{\mathrm{d}t_{w_n}(\theta)}{\mathrm{d}\theta}\mathrm{d}\theta q_{w_{ko}}(t)q_{w_{lp}}(t)q_{w_{jn}}(t)\\
&-\frac{\ell}{4R^3}\int_{-1}^{1}f_{w_j}(\xi)f_{w_k}(\xi)f_{w_l}(\xi)f_{w_j}(\xi)A_{22}(\xi)\mathrm{d}\xi\int_0^{2\pi}\frac{\mathrm{d}t_{w_m}(\theta)}{\mathrm{d}\theta}\frac{\mathrm{d}t_{w_o}(\theta)}{\mathrm{d}\theta}\frac{\mathrm{d}t_{w_p}(\theta)}{\mathrm{d}\theta}\frac{\mathrm{d}t_{w_n}(\theta)}{\mathrm{d}\theta}\mathrm{d}\theta q_{w_{ko}}(t)q_{w_{lm}}(t)q_{w_{jn}}(t)\\
&-\frac{1}{R^2}\int_{-1}^{1}f_{w_i}(\xi)f_{w_k}(\xi)f_{w_l}(\xi)\frac{\mathrm{d}f_{w_j}(\xi)}{\mathrm{d}\xi}A_{26}(\xi)\mathrm{d}\xi\int_0^{2\pi}\frac{\mathrm{d}t_{w_m}(\theta)}{\mathrm{d}\theta}\frac{\mathrm{d}t_{w_o}(\theta)}{\mathrm{d}\theta}\frac{\mathrm{d}t_{w_p}(\theta)}{\mathrm{d}\theta}t_{w_n}(\theta)\mathrm{d}\theta q_{w_{ko}}(t)q_{w_{lp}}(t)q_{w_{jn}}(t)
\end{aligned}
\tag{A3}
$$

$$= \frac{R\ell}{2}\int_{-1}^{1}\int_{0}^{2\pi} f_{w_i}(\xi)\, t_{w_m}(\theta)\, p_z(x,\theta,t)\,\mathrm{d}\theta\mathrm{d}\xi + \rho h \frac{R\ell}{2}\int_{-1}^{1} f_{w_i}(\xi)\, f_{w_j}(\xi)\mathrm{d}\xi \int_{0}^{2\pi} t_{w_m}(\theta)\, t_{w_n}(\theta)\mathrm{d}\theta \frac{\mathrm{d}^2 q_{w_{jn}}(t)}{\mathrm{d}t^2}$$

Appendix 2

Verification of the Model

Some of the numerical tests carried out in order to verify the model implemented are presented in this appendix. The first two tests concern the natural frequencies of vibration of a constant stiffness shell. The third test relates to the critical freestream pressure. The shell characteristics are provided in the tables' captions.

In Table 5, non-dimensional values of natural frequencies computed using the present model with diverse numbers of shape functions are compared with published results. Results labelled as "Present" were computed with the full model. In between brackets is the relative difference to the values with 21 unidimensional shape functions (*usf*) per displacement component. All modes exhibit one longitudinal wave; the number of circumferential waves is denoted by n. The radius, R, was set to 1 m. A complete convergence test would require independently evaluating the number of functions of ξ and of θ for each displacement component; this was not carried out. Instead, sixteen, nineteen, or twenty-one unidimensional shape functions—both in ξ and in θ—were used for each of the three displacement components to verify whether reasonable convergence had been achieved. The circumferential functions are from Eqs. (22) and (23). In this section, the constant function of Eqs. (23) is not used, so we have $t_{v_k}(\theta) = \sin(k\theta)$, $k \geq 1$. Six digits are shown after the decimal point to better illustrate the differences, but the number of relevant digits is lower in most cases.

Table 5 shows that with 16 unidimensional shape functions in ξ and 16 in θ, for each displacement component, the first ten natural frequencies of vibration values are nearly

Table 5 Comparison of frequency parameters $\Omega = \omega R\sqrt{\rho/E_{22}}$ of a clamped–clamped circular cylindrical shell, [0º, 90º, 0º] and: $\ell/R = 5$, $h/R = 0.002$, $E_{22} = 7.6$ GPa, $E_{11}/E_{22} = 2.5$, $G_{12} = 4.1$ GPa, $\nu_{12} = 0.26$, $\rho = 1643$ kg/m^3

n	Jin et al. [53]	Xie et al. [54]	Present 16 *usf*	Present 19 *usf*	Present 21 *usf*
1	0.303609	0.303318	0.303168 (0.009%)	0.303145 (0.001%)	0.303142
2	0.166909	0.167527	0.166909 (0.025%	0.166873 (0.003%)	0.166868
3	$0.99194\cdot10^{-1}$	$0.99667\cdot10^{-1}$	$0.991941\cdot10^{-1}$ (0.037%)	$0.991626\cdot10^{-1}$ (0.005%)	$0.991577\cdot10^{-1}$
4	$0.64400\cdot10^{-1}$	$0.64699\cdot10^{-1}$	$0.643998\cdot10^{-1}$ (0.042%)	$0.643762\cdot10^{-1}$ (0.006%)	$0.643725\cdot10^{-1}$
5	$0.46171\cdot10^{-1}$	$0.46345\cdot10^{-1}$	$0.461709\cdot10^{-1}$ (0.041%)	$0.461546\cdot10^{-1}$ (0.006%)	$0.461520\cdot10^{-1}$
6	$0.38128\cdot10^{-1}$	$0.38222\cdot10^{-1}$	$0.381275\cdot10^{-1}$ (0.031%)	$0.381172\cdot10^{-1}$ (0.004%)	$0.381155\cdot10^{-1}$
7	-	-	$0.375581\cdot10^{-1}$ (0.018%)	$0.375523\cdot10^{-1}$ (0.002%)	$0.375514\cdot10^{-1}$
8	-	-	$0.422909\cdot10^{-1}$ (0.008%)	$0.422879\cdot10^{-1}$ (0.001%)	$0.422874\cdot10^{-1}$
9	-	-	$0.504320\cdot10^{-1}$ (0.004%)	$0.504304\cdot10^{-1}$ (0.001%)	$0.504301\cdot10^{-1}$
10	-	-	$0.608320\cdot10^{-1}$ (0.002%)	$0.608311\cdot10^{-1}$ (0.0002%)	$0.608310\cdot10^{-1}$

Table 6 Convergence and condensation[1,2] of present model; frequency parameters $\Omega = \omega R\sqrt{\rho/E_{22}}$ of a CC circular cylindrical shell, [0º, 90º, 0º] and: $\ell/R = 5$, $h/R = 0.002$, $E_{22} = 7.6$ GPa, $E_{11}/E_{22} = 2.5$, $G_{12} = 4.1$ GPa, $\nu_{12} = 0.26$, $\rho = 1643$ kg/m^3

	19 unidimensional shape functions			
n	Full model	Reduced model 1	Reduced model 2	Relative difference full-reduced 1/full-reduced 2
1	0.303145	0.303596	0.4128355	0.15%/36%
2	0.166873	0.167109	0.1863088	0.14%/12%
3	$0.991626\cdot10^{-1}$	$0.992422\cdot10^{-1}$	0.104589	0.080%/5.5%
4	$0.643762\cdot10^{-1}$	$0.644032\cdot10^{-1}$	$0.663880\cdot10^{-1}$	0.042%/3.1%
5	$0.461546\cdot10^{-1}$	$0.461649\cdot10^{-1}$	$0.470814\cdot10^{-1}$	0.022%/2.0%
6	$0.381172\cdot10^{-1}$	$0.381220\cdot10^{-1}$	$0.386492\cdot10^{-1}$	0.013%/1.4%
7	$0.375523\cdot10^{-1}$	$0.375552\cdot10^{-1}$	$0.379373\cdot10^{-1}$	0.008%/1.0%
8	$0.422879\cdot10^{-1}$	$0.422899\cdot10^{-1}$	$0.426196\cdot10^{-1}$	0.005%/0.78%
9	$0.504304\cdot10^{-1}$	$0.504320\cdot10^{-1}$	$0.507428\cdot10^{-1}$	0.003%/0.62%
10	$0.608311\cdot10^{-1}$	$0.608324\cdot10^{-1}$	$0.611362\cdot10^{-1}$	0.002%/0.50%

1 – longitudinal inertia neglected

2 – membrane inertia neglected

equal to the reference values computed using 21 functions. The present results are also similar to the values published in [53] and [54]. Although independently implemented, the linear part of the present model is based on the same hypothesis of reference [31], hence the values also agree with the ones there given, which are not included in the table.

Table 6 addresses the same shell, but for the purpose of verifying the impact of the two types of condensation proposed in Sect. "Equations of Motion – reduced-order Models". The values obtained for the natural frequencies demonstrate that the longitudinal inertia can be neglected, if one accepts to add an error below 0.2%. On the other hand, the circumferential inertia (inertia related to accelerations $\ddot{v}$) is important in modes with a small number of circumferential waves. This is particularly easy to understand in mode $n=1$: the mode shape represented in Fig. 15 shows that displacements (hence also

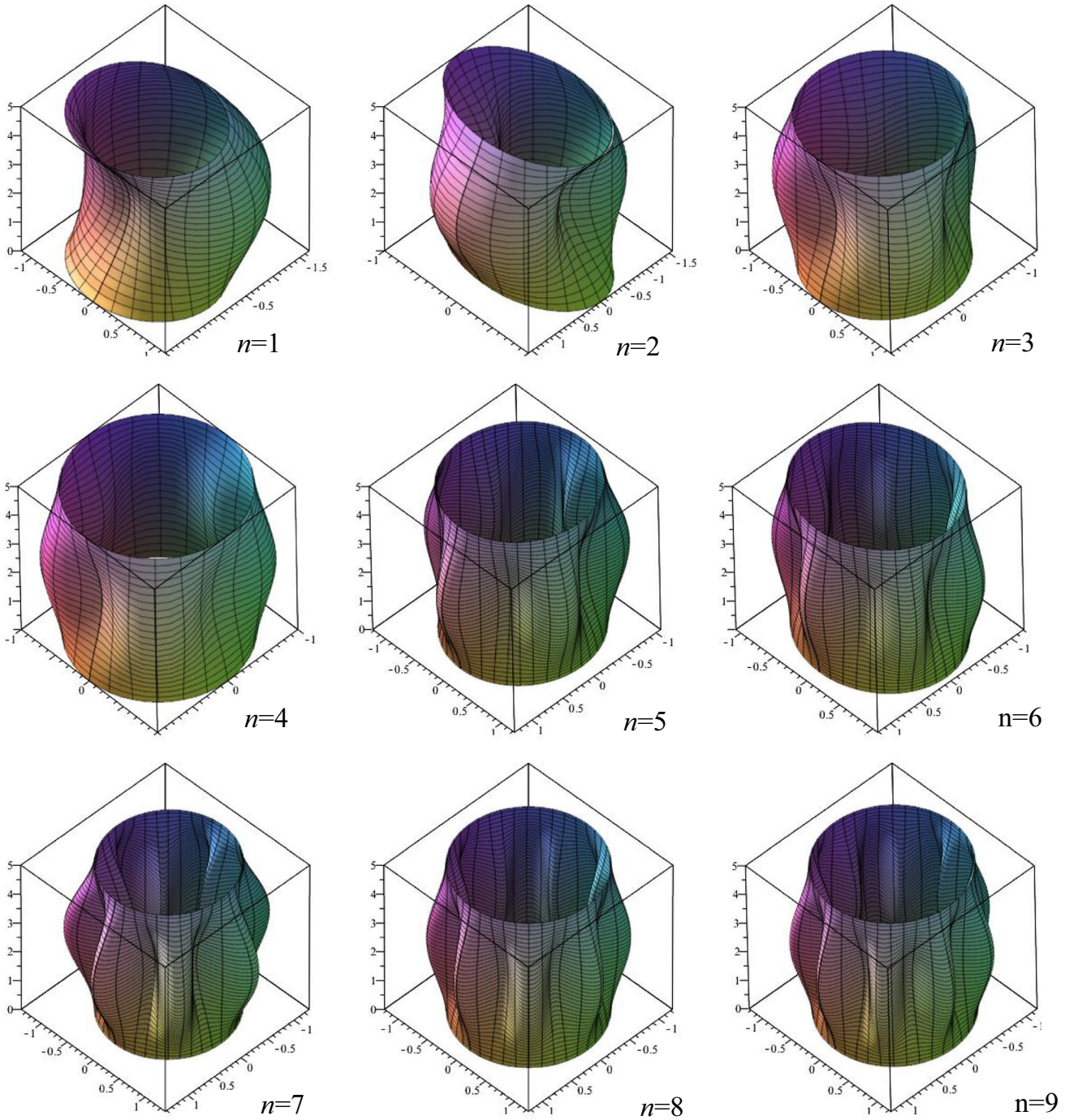

Fig. 15 Mode shapes of vibration, full model, natural frequencies on Table 6

Table 7 Critical freestream pressure p_{crit} for the occurrence of flutter for SS boundary conditions of circular cylindrical shells with the following parameters: $G_{12}=E_{11}/[2\cdot(1+\nu_{12})]$, $h=0.0001015$ m, $R=0.203$ m, $\rho=8900$ kg/m^3, $M=3$, $a_\infty=213$ m/s, $\gamma=1.4$, $\ell=0.381$ m, $\nu_{12}=0.35$, $E_{11}=E_{22}=110\cdot10^9$ GPa, shell originally analysed in [4]

Reference	p_{crit} [Pa]	n_{crit}
Olson and Fung [4]	3940	25
Ganapathi et al. [55]	3875	26
Amabili [2]	3628	25
Avramov et al. [56]	3599	26
Cachulo et al. [31]; $p_m=p_o=10$, $p_t=30$ (full model)	3864	25
Present model (without membrane inertia)	3868	25

accelerations) in direction y (Fig. 1) are of approximately the order of magnitude of displacements in the transverse direction. Only for $n\geq4$ are the differences between reduced model 1 and the full model lower than 5%.

Table 7 addresses a shell very often analysed in the literature. The properties used are given in the table caption and were the ones employed in a number of references, where less significant digits were discarded in the conversion from the imperial to the metric system of units of the earliest reference [4]. The simple supports allow for longitudinal displacement in the boundaries, as detailed in [55]. The present model does not include membrane inertia; the number of functions used is $p_w=10$, $p_{tw}=13$; starting number for circumferential functions = 17. The value of the critical freestream pressure is close to the ones available in the literature, including the experimental ones of [4].

Using very detailed models, flutter modes with longitudinal waves of very short wavelength were found in some cylindrical shells in the course of this work. These flutter modes appear to have been overlooked in the literature. We decided to focus on the flutter modes with a number of waves near the one found in the laboratory by Olson and Fung [3], because these have been experimentally confirmed and because our shell model neglects transverse shear and rotary inertia, and may lose accuracy if the wave length is too short.

Figure 16 shows the evolution of the transverse displacement of a point of Olson and Fung's [4] shell in time and the said transverse displacement versus the respective velocity. The plots were obtained with the non-linear model represented by Eqs. (37); the initial conditions are null velocity and a small displacement of the shell with the flutter mode shape corresponding to the critical point of Table 7. The velocity in the vertical axis of Fig. 16 (b), is non-dimensionalised using $2\pi\omega_{\ell_1}h$, where ω_{ℓ_1} is the first natural frequency of vibration of the shell, in rad/s. The plots show that, after the critical freestream pressure, the shell undergoes a limit cycle, harmonic, oscillation. Harmonic oscillations after flutter, similar to the ones shown in the figure, are also presented in [4, 56].

Another test in the linear regime was carried out for verification purposes: determining the critical free flow pressure of a variable stiffness composite laminated shell already analysed in [31]. The shell has 12 layers and the following geometric properties (m): $R=0.203$; $h=0.10150\cdot10^{-3}$, $\ell=0.406$. This extremely thin thickness, chosen because it is not far from the reference work by Olson and Fung [4], is rather academic in a 12 layered VS shell, with today's technology. The particular shell layup analysed can be written as $[3\,(<\Theta_0,\,\Theta_1>,<-\Theta_0,-\Theta_1>)]_s$, $\Theta_0,=40^o,\Theta_1=80^o$. With 12 unidimensional shape functions per displacement component (432 dof, full model), using the reduced model without membrane inertia, the critical free flow pressure, p_{crit}, is 2358.9 ± 0.1 Pa. Using the full model, the value attained is

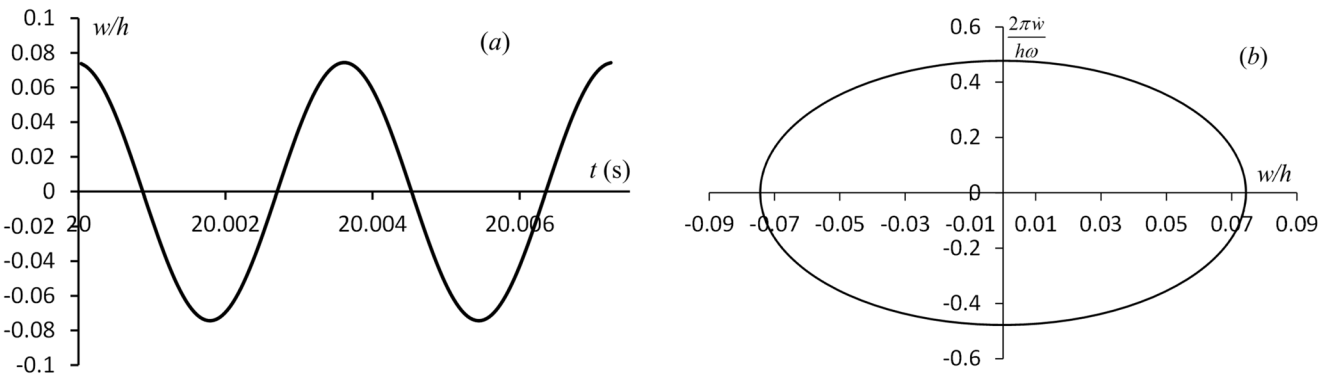

Fig. 16 (**a**) Transverse displacement versus time and versus (**b**) velocity. Point $x=0.775\,\ell$m, $\theta=0$ rad. Pressure $p_\infty=4000$ Pa; remaining conditions as in the caption of Table 7

2365.75 ± 0.25 Pa. Both values are close to the value found in [31], 2368 Pa. The model used in [31] corresponds to the linear part of the present full model, but was implemented separately by another researcher.

Acknowledgements The first author would like to acknowledge the support of Reitoria da Universidade do Porto para Mobilidade Docente, in the framework of the agreement between this university and Bank Santander, grant code ASM22AC0637, as well as the Applied Mechanics Section, DEMec, FEUP for conceding a sabbatical license that turned this work possible.

Data Availability Data will be made available upon reasonable request. The authors may decide to keep parts of their work—e.g. computational codes—for their sole use.

Declarations

Conflict of interest On behalf of all authors, the corresponding author states that there is no conflict of interest.

References

1. Dowell H (2015) A modern course in aeroelasticity. Springer, Heidelberg
2. Amabili M (2008) Nonlinear vibrations and stability of shells and plates. Cambridge University Press, Cambridge, United Kingdom
3. Olson MD, Fung YC (1966) Supersonic flutter of circular cylindrical shells subjected to internal pressure and axial compression. AIAA J 4:858–864
4. Olson MD, Fung YC (1967) Comparing theory and experiment for the supersonic flutter of circular cylindrical shells. AIAA J 5:1849–1856
5. Nichols JJ (1969) Final report: Saturn V: Panel flutter qualification test. Washington, NASA-TN-D-5439, D.C.: National Aeronautics and Space Administration. https://ntrs.nasa.gov/citations/19690029423
6. Barr GW, Stearman RO (1970) Influence of a supersonic flowfield on the elastic stability of cylindrical shells. AIAA J 8:993–1000
7. Ghiasi H, Fayazbakhsh K, Pasini D, Lessard L (2010) Optimum stacking sequence design of composite materials Part II: variable stiffness design. Compos Struct 93:1–13
8. Ribeiro P, Akhavan H, Teter A, Warminski J (2014) A review on the mechanical behaviour of curvilinear fibre composite laminated panels. J Compos Mater 48:2761–2777. https://doi.org/10.1177/0021998313502066
9. Lozano GG, Tiwari A, Turner C, Astwood S (2016) A review on design for manufacture of variable stiffness composite laminates. Proc Inst Mech Eng Part B J Eng Manuf 230:981–992. https://doi.org/10.1177/0954405415600012
10. Albazzan MA, Harik R, Tatting BF, Gürdal Z (2019) Efficient design optimization of nonconventional laminated composites using lamination parameters: a state of the art. Compos Struct 209:362–374. https://doi.org/10.1016/j.compstruct.2018.10.095
11. Sobhani Aragh B, Borzabadi Farahani E, Xu BX, Ghasemnejad H, Mansur WJ (2021) Manufacturable insight into modelling and design considerations in fibre-steered composite laminates: State of the art and perspective. Comput Methods Appl Mech Eng 379:113752. https://doi.org/10.1016/j.cma.2021.113752
12. Tatting BF (1998) Analysis and design of variable stiffness composite cylinders [Ph.D.]: Virginia Polytechnic Institute and State University, USA
13. Blom AW (2010) Structural performance of fiber-placed, variable-stiffness composite conical and cylindrical shells [Ph.D.]: Delft University of Technology, The Netherlands
14. Blom AW, Setoodeh S, Hol J, Gurdal Z (2008) Design of variable-stiffness conical shells for maximum fundamental eigenfrequency. Comput Struct 86:870–878
15. Rouhi M, Ghayoor H, Fortin-Simpson J, Zacchia TT, Hoa SV, Hojjati M (2018) Design, manufacturing, and testing of a variable stiffness composite cylinder. Compos Struct 184:146–152
16. Labans E, Bisagni C (2019) Buckling and free vibration study of variable and constant-stiffness cylindrical shells. Compos Struct 210:446–457. https://doi.org/10.1016/j.compstruct.2018.11.061
17. Almeida JHS, Bittrich L, Jansen E, Tita V, Spickenheuer A (2019) Buckling optimization of composite cylinders for axial compression: a design methodology considering a variable-axial fiber layout. Compos Struct. https://doi.org/10.1016/j.compstruct.2019.110928
18. Wang Z, Almeida JHS, Ashok A, Wang Z, Castro SGP (2022) Lightweight design of variable-angle filament-wound cylinders combining Kriging-based metamodels with particle swarm optimization. Struct Multidiscip Optim. https://doi.org/10.1007/s00158-022-03227-8
19. Kumar P, Hirwani CK (2025) HSDT and FE based nonlinear formulation of variable stiffness composite laminated shell panel for investigating nonlinear dynamic behaviour. J Vib Eng Technol. https://doi.org/10.1007/s42417-025-01988-2
20. Amabili M, Pellicano F (2001) Nonlinear supersonic flutter of circular cylindrical shells. AIAA J 39:564–573
21. Amabili M, Pellicano F (2002) Multimode approach to nonlinear supersonic flutter of imperfect circular cylindrical shells. J Appl Mech 69:117–129
22. Sabri F, Lakis AA (2010) Finite element method applied to supersonic flutter of circular cylindrical shells. AIAA J 48:73–81
23. ChenJ, Li Q-S (2017) Nonlinear aeroelastic flutter and dynamic response of composite laminated cylindrical shell in supersonic air flow. Compos Struct 168:474–484. https://doi.org/10.1016/j.compstruct.2017.02.019
24. Ben-Youssef Y, Kerboua Y, Lakis AA (2022) Analysis of nonlinear vibrations of thin cylindrical shells subjected to supersonic flow. Thin-Walled Structures. https://doi.org/10.1016/j.tws.2022.108969
25. Jutte CV, Wieseman CD, Lovejoy AE, Stanford B (2020) Static loads testing of a high aspect ratio tow-steered wingbox. AIAA 2020-0243. AIAA Scitech 2020 Forum. https://doi.org/10.2514/6.2020-0243
26. Brooks TR, Martins JRRA, Kennedy GJ (2019) High-fidelity aerostructural optimization of tow-steered composite wings. J Fluids Struct 88:122–147. https://doi.org/10.1016/j.jfluidstructs.2019.04.005
27. Stanford BK, Jutte CV (2014) Aeroelastic Tailoring via tow steered composites, NASA/TM–2014–218517. National Aeronautics and Space Administration, Virginia. https://ntrs.nasa.gov/api/citations/20140012777/downloads/20140012777.pdf
28. Akhavan H, Ribeiro P (2018) Aeroelasticity of composite plates with curvilinear fibres in supersonic flow. Compos Struct 194:335–344. https://doi.org/10.1016/j.compstruct.2018.03.101
29. Akhavan H, Ribeiro P (2019) Reduced-order models for nonlinear flutter of composite laminates with curvilinear fibers. AIAA J 57:3026–3039. https://doi.org/10.2514/1.J057755
30. Akhavan H, Ribeiro P (2020) Stability and bifurcations in oscillations of composite laminates with curvilinear fibres under a supersonic airflow. Nonlinear Dyn. https://doi.org/10.1007/s11071-020-05838-6
31. Cachulo D, Akhavan H, Ribeiro P (2023) Supersonic flutter of variable stiffness circular cylindrical shells. Compos Struct. https://doi.org/10.1016/j.compstruct.2023.116927
32. Akhavan H, Ribeiro P (2022) Nonlinear flutter of composite laminates with curvilinear fibres using a full linearized aerodynamic

theory. J Fluids Struct. https://doi.org/10.1016/j.jfluidstructs.2022.103756
33. Moreira JA, Moleiro F, Araújo AL, Pagani A (2024) Layerwise models for supersonic flutter analysis of viscoelastic sandwich panels with curvilinear fibre composite skins. J Sound Vib. https://doi.org/10.1016/j.jsv.2023.118182
34. Nayfeh AH, Balachandram B (1994) Applied nonlinear dynamics: analytical, computational, and experimental methods. John Wiley and Sons, New York
35. Dym CL, Shames IH (2013) Solid mechanics: Springer, New York
36. Meirovitch L (1980) Computational methods in structural dynamics. Springer, Dordrecht
37. Amabili M, Reddy JN (2010) A new non-linear higher-order shear deformation theory for large-amplitude vibrations of laminated doubly curved shells. Int J Non-Linear Mech 45:409–418
38. Qatu MS (2004) Vibration of laminated shells and plates: Academic Press
39. Ventsel E, Krauthammer T (2001) Thin plates and shells: theory: analysis, and applications: CRC Press, New York. https://doi.org/10.1201/9780203908723
40. Li F-M, Yao G (2013) 1/3 subharmonic resonance of a nonlinear composite laminated cylindrical shell in subsonic air flow. Compos Struct 100:249–256. https://doi.org/10.1016/j.compstruct.2012.12.035
41. Croft K, Lessard L, Pasini D, Hojjati M, Chen J, Yousefpour A (2011) Experimental study of the effect of automated fiber placement induced defects on performance of composite laminates. Compos Part A Appl Sci Manuf 42:484–491
42. Kim BC, Weaver PM, Potter K (2014) Manufacturing characteristics of the continuous tow shearing method for manufacturing of variable angle tow composites. Compos Part A Appl Sci Manuf 61:141–151
43. Han W, Petyt M, Hsiao KM (1994) An investigation into geometrically nonlinear analysis of rectangular laminated plates using the hierarchical finite element method. Finite Elem Anal Des 18:273–288
44. Bardell NS (1989) The application of symbolic computing to the hierarchical finite element method. Int J Numer Methods Eng 28:1181–1204
45. Ribeiro P (2001) Hierarchical Finite Element Analyses of Geometrically Non-Linear Vibration of Beams and Plane Frames. J Sound Vib 246:225–244
46. Gonçalves EH, Ribeiro P (2021) Modes of vibration of single- and double-walled CNTs with an attached mass by a non-local shell model. J Vib Eng Technol 10:375–393. https://doi.org/10.1007/s42417-021-00381-z
47. Camacho P, Ribeiro P, Akhavan H (2025) An hp-finite element for vibration analysis of laminates reinforced with curvilinear fibres. Finite Elem Anal Des. https://doi.org/10.1016/j.finel.2024.104280
48. Ribeiro P (2009) On the influence of membrane inertia and shear deformation on the geometrically non-linear vibrations of open, cylindrical, laminated clamped shells. Compos Sci Technol 69:176–185
49. Petyt M (2010) Introduction to Finite Element Vibration Analysis, 2nd edn. Cambridge University Press, Cambridge
50. Antunes AM, Ribeiro P, Dias Rodrigues J, Akhavan H (2020) Modal analysis of a variable stiffness composite laminated plate with diverse boundary conditions: experiments and modelling. Compos Struct 239:111974. https://doi.org/10.1016/j.compstruct.2020.111974
51. Waldhart C (1996) Analysis of Tow-Placed, Variable-Stiffness Laminates. Virginia Polytechnic Institute and State University, Blacksburg, Virginia, USA
52. The MathWorks Inc. lyapunovExponent. MATLAB Help Center, USA (2018). https://www.mathworks.com/help/predmaint/ref/lyapunovexponent.html
53. Jin G, Ye T, Chen Y, Su Z, Yan Y (2013) An exact solution for the free vibration analysis of laminated composite cylindrical shells with general elastic boundary conditions. Compos Struct 106:114–127
54. Xie X, Jin G, Yan Y, Shi SX, Liu Z (2014) Free vibration analysis of composite laminated cylindrical shells using the Haar wavelet method. Compos Struct 109:169–177
55. Ganapathi M, Varadan TK, Jijen J (1994) Field-consistent element applied to flutter analysis of circular cylindrical shells. J Sound Vib 171:509–527
56. Avramov KV, Chernobryvko M, Uspensky B, Seitkazenova KK, Myrzaliyev D (2019) Self-sustained vibrations of functionally graded carbon nanotubes-reinforced composite cylindrical shells in supersonic flow. Nonlinear Dyn 98:1853–1876. https://doi.org/10.1007/s11071-019-05292-z